European Polymer Journal 215 (2024) 113211

Contents lists available at ScienceDirect

European Polymer Journal

journal homepage: www.elsevier.com/locate/europolj

The effect of PEGylation components on drug release behavior of targeted reduced graphene oxide based drug delivery system

Ezgi Basavci [a], Erhan Demirel [a,b], Mohamad Elhassan [a], Yasemin Yuksel Durmaz [a,b,*]

[a] School of Engineering and Natural Sciences, Department of Biomedical Engineering, Istanbul Medipol University, 34810, Istanbul, Turkey
[b] Research Institute of Health Science and Technologies (SABITA), Istanbul Medipol University, 34810, Istanbul, Turkey

ARTICLE INFO

Keywords:
Graphene Oxide
PEGylation
π-π interaction
Biocompatible
Targeting Drug Delivery System
Drug Release

ABSTRACT

Reduced graphene oxide (rGO) is a restored, defect-free version of graphene oxide (GO) with regained graphene-like properties but encounters challenges in biomedical applications due to its low solubility. Especially for drug release applications, rGO's stronger π-π interaction of rGO compared to GO leads to low release, often demanding novel approaches for enhancement. The recently developed PEGylation method utilizes a copolymer with tunable PEG chain length and density for the PEGylation of GO simultaneously reduced to rGO, resulting in water-dispersible and biocompatible rGO-based nanoplatforms. This copolymer integrates functional monomers and enhances treatment options. Herein, we investigated how these PEGylation components and their incorporation order impact rGO's drug release behavior. A series of copolymers, (P(PEGMA-*co*-AzPMA-*co*-MMA-*co*-PMA), with different PEG brushes and azide groups, were synthesized via atom transfer radical polymerization. We explored the impact of ionic azide groups on drug release by comparing the azide-containing and azide-capped copolymers. Moreover, copolymers containing 500 or 2000 Da PEG brushes were compared to assess their role as a coating layer or diffusion barrier on drug release. Doxorubicin, a hydrophobic anticancer agent, was loaded onto the rGO surface before or after peptide-based targeting agent (EPPT1) conjugation. The results showed that the drug release behavior of 500 or 2000 Da PEG brushes containing rGO surfaces are different due to the density of PEG coating which makes the effect of azide groups not always visible. Incorporating the targeting peptide before drug loading was found to be optimal. The pH-dependent release profiles revealed 49 % and 44 % release from the rGO surface for the shorter and longer PEG brushes, respectively. Tuning the PEGylation components may further influence the release behavior.

1. Introduction

Flat monolayered carbon allotrope graphene (G) and its various types have gained interest since their discovery in 2004 [1]. Graphene and its derivatives have a two-dimensional hexagonal organization of a thick sp^2 hybridized carbon atom, providing superior properties such as high electron mobility and electrical conductivity [2] Their wide and adjustable surface for facile functionalization makes them an attractive option for a variety of biological applications such as multi-purpose carriers [3], tissue engineering scaffolds [4], and composite materials [3,5]. The widely used alternatives of graphene are water soluble, oxygen-rich graphene oxide (GO) with surface defects, and reduced graphene oxide (rGO), which is the restored version by chemical or thermal reduction. Although GO features functional groups such as hydroxyl, epoxy, and carbonyl groups, they are often preferred for biological applications [2] and tend to interact with salts, ions, and biomolecules under physiological conditions. This interaction can lead to flocculation and aggregation of adequately dispersed GO, potentially impacting its cytotoxicity, which depends on its size, shape, and concentration [6,7]. It is also known that these oxygen-containing functional groups can contribute to reactive oxygen generation, which is one of the toxicity mechanisms of graphene derivatives [8,9]. Conversely, rGO exhibits superior physical and optical characteristics compared to those of GO. With a less defective surface, rGO maintains its capability for non-covalent bonding, including π-π stacking, Van der Waals forces, electrostatic interactions, and hydrogen bonding [10–12]. However, this derivative suffers from poor water solubility, which limits its use in biological applications. Despite these superior features, the basal plane of GO is largely hydrophobic, which leads to the absorption of proteins and hydrophobic molecules. This phenomenon results in surface

* Corresponding author.
E-mail address: ydurmaz@medipol.edu.tr (Y. Yuksel Durmaz).

https://doi.org/10.1016/j.eurpolymj.2024.113211
Received 28 March 2024; Received in revised form 21 May 2024; Accepted 7 June 2024
Available online 9 June 2024

chemistry inconsistencies, instability, and aggregating adequately dispersed GO derivatives under physiological conditions [13]. A common strategy to overcome these problems is to coat the surface with various natural and synthetic polymers that have been used as coatings or stabilizing agents, such as poly(ethylene glycol) (PEG), hyaluronic acid, dextran, and chitosan [14–17]. Among these, PEG, as an FDA-approved polymer, has been extensively employed to increase the biocompatibility and water dispersibility [18,19] of not only graphene derivatives as well as other carbon-based materials. For instance, it was shown that the cytotoxicity of carbon nanotubes significantly decreased with an increasing degree of PEGylation at the surface [20] since PEG as a coating material provides a hydrated layer that decreases the protein and nutrition adsorption of carbon-based surfaces. Moreover, graphdiyne, a new carbon-based nanomaterial, was modified with a PEG-containing polymer that enabled graphdiyne to cross the blood–brain barrier [21], and our group has developed an effective PEGylation method yielding water-dispersible rGO [22]. Our study utilized a novel copolymer comprising poly(ethylene glycol) methyl ether methacrylate (PEGMA), methyl methacrylate (MMA), and 1-pyrenemethyl methacrylate (PMA) (P(PEGMA-*co*-MMA-*co*-PMA)), synthesized via atom transfer radical polymerization (ATRP), with a molecular weight below 50 KDa to facilitate renal excretion and minimize potential toxicity, while utilizing a branched structure to prolong circulation time in the blood [23]. Essentially, this study is a novel technique that incorporates tunable PEG brushes to ensure aqueous dispersibility alongside multiple pyrene groups to facilitate π-π interactions with the surface of rGO, which is simultaneously reduced from GO. Instead of edge modification, distributed PEG brushes on the wide graphene surface reduce, the chance of nutrient adsorption by the surface, and simultaneous reduction provides defect-free rGO with fewer oxygen-containing groups. Therefore, the obtained water-dispersible rGO has better biocompatibility because it addresses most of the cytotoxicity mechanisms of graphene by lowering reactive oxygen species, less interaction with cell nutrition, and better stability in cell medium [22]. It is common in the literature to use pyrene or other aromatic moieties as anchoring molecules to coat carbon-based materials through physical interactions to tune their surface properties [24]. However, our study clearly showed that the presence of multiple pyrene units in the copolymer increased the coating efficiency on the rGO surface. MMA monomers in the copolymer were utilized as chain extenders to distribute the pyrene as π-π interacting anchoring group throughout the polymer chain. Furthermore, our group showed that this copolymer could be tailored by carrying functional monomers to combine different treatments on the surface of the rGO nanoplatform. The azide group was introduced into the copolymer and used for the conjugation of the cationic copolymer for siRNA condensation and as a targeting agent for selective cellular entry. It was shown that doxorubicin (Dox), as an anticancer agent, could be successfully loaded onto the resulting nanoplatform as a targeted dual drug delivery agent [25].

Precise and comprehensive delivery of hydrophobic drugs is an indispensable aspect of efficient cancer therapy. Even though drugs such as doxorubicin, paclitaxel, epirubicin, curcumin, and 5-fluorouracil can be loaded with high drug loading efficiency on a large graphene surface and secure the loaded drug during circulation, it is a known fact that graphene-based drug delivery systems can have various drug release profiles that can be affected by surface components [26]. Although there are many examples of Dox-loaded PEGylated GO surfaces in the literature [27–30], there are few studies that provide information about the effect of PEG brush length on the drug release behavior of the rGO surface. Mahdavi et al. computationally showed that the length of PEG chains on the graphene surface affects the localization of Dox on the GO surface since increasing PEG chain length creates a hydrated layer and forces Dox to migrate to the non-PEGylated part of the GO. Once GO is coated with short PEG chains (500 Da), these chains fold over the GO surface, and Dox is absorbed in the uncovered region of GO. In the case of longer PEG chains (1000 Da), chains are mostly protruding, and a lack of an uncovered region causes the aggregation of Dox within the PEG chains [31]. Therefore, the effect of coating (PEGylation) components and the order of incorporation of these components onto the graphene surface need to be investigated for the previously proposed PEGylation method, which can be tuned to the graphene surface with PEG chains of different lengths and azide groups to further target peptide conjugation [22,25]. Because our PEGylation method uses a multifunctional copolymer for coating instead of a single PEG chain, the backbone of the copolymer along with pyrene and azide groups is expected to be closer to the rGO surface. Dox is expected to interact with the rGO surface through π-π stacking, hydrophobic interaction, and hydrogenbonding. Because of the protonation of Dox in an acidic environment, it carries a positive charge, which weakens hydrogenbonding. Additionally, it can interact with charged azide groups, which functionalize the coated copolymer. Our recently published study supported the possibility of electrostatic interactions by enhancing drug release when the cationic copolymer was conjugated to the copolymer and coated on the rGO surface [25]. Furthermore, the order of targeting agent conjugation and drug loading may be a parameter contributing to drug release.

To address all these hypotheses, a series of copolymers similar to previous study but including azide containing functional monomer, poly [(poly(ethylene glycol methacrylate))–*co*-(3-azido propyl methacrylate)–*co*-(methyl methacrylate)–*co*-(1-pyrene methacrylate)] (P(PEGMA-*co*-AzPMA-*co*-MMA-*co*-PMA), with different numbers of PEG brushes and azide groups were synthesized via ATRP. The main purpose of the azide group was to accommodate the functionalization for further application. However, it was revealed that the presence and quantity of azide groups affected drug release, highlighting one of the key findings of our study. Moreover, copolymers containing PEG brushes with different lengths (500 or 2000 Da) were compared to determine the brush length effect because the density of PEG content as a diffusion barrier may affect the drug release of nanoplatforms. As in the original PEGylation method, multiple pyrene units were used to increase π-π interactions and provide an effective coating, while the MMA monomer was used as a chain extender to distribute functional monomers along the chain. Dox was loaded to the rGO surface before and after targeting agent conjugation using the azide group as a functionalization tool, followed by capping the remaining azide groups with propargyl alcohol. EPPT1 peptide was selected as a peptide-based active targeting agent that recognizes the underglycosylated mucin-1 antigen (uMUC-1) [32] in different cancer types, such as breast cancer, which is overexpressed in $>$ 90 % of cases. Herein, all the components were introduced during the coating of the rGO surface with functional copolymers are commonly used tools such as PEGylation, targeting agent conjugation, and drug loading. This study will shed light on the effect of PEG brush length and density on drug release or whether conjugation of the targeting agent before or after drug loading affects drug release. Moreover, the effect of azide groups on drug release behavior was investigated by comparing the drug release profiles of the coated rGO with well-defined copolymers containing comparable PEG brushes and azide groups at pH 5.5 and 7.4, to mimic tumor and physiological conditions, respectively. The anticancer activity of rGO based nanoplatforms was observed based on their effect on the viability of MCF-7 breast cancer cells using a resazurin assay. Moreover, the difference between the cellular uptake of targeted and non-targeted nanoplatforms was observed in the MCF-7 cell line using confocal microscopy and fluorescence-activated cell sorting (FACS). Collectively, the results showed that the presence and increasing number of azide groups increased the drug release of more brush containing shorter (500 Da) PEG coated surface and less brush containing longer PEG(2000 Da) coated rGO surface. Increasing the PEG chain length provided better water dispersibility and biocompatibility to the nanoplatform. The best order to incorporate the peptide-based targeting agent into the nanoplatform was before drug loading.

2. Experimental part

2.1. Materials

Methyl methacrylate (MMA, Sigma-Aldrich, 99 %), poly(ethylene glycol) methyl ether methacrylate (PEGMA, 500 and 2000 Da, Sigma-Aldrich), 1-pyrenemethyl methacrylate (PMA, Sigma-Aldrich, 99 %), *N,N,N',N'',N''*-pentamethyldiethylenetriamine (PMDETA, Sigma-Aldrich, 99 %) were passed through a basic alumina column to remove inhibitor prior to use. Copper (I) bromide (CuBr, Sigma-Aldrich, 98 %), ethyl 2-bromo-2-methyl propionate (EiBr, Sigma-Aldrich, 98 %), graphene oxide (GO, Sigma-Aldrich, 4 mg/mL dispersion in H_2O), 3-azido-1-propanol (Sigma-Aldrich, 96 %), methacryloyl chloride (Sigma-Aldrich), triethylamine (J.T. Baker), doxorubicin hydrochloride (Dox, Sigma-Aldrich, 98 %), propargyl alcohol (Sigma-Aldrich, 99 %), EPPT1 (YCAREPPTRTFAYWG, C terminus capped, N terminus free > 95 %, Metabion International AG, Germany), Triton™ X-100 (Sigma-Aldrich), sodium chloride anhydrous (NaCl, Wisent Bioproducts, 99 %), phosphate buffer solution (PBS, Multicell, Wisent Inc.), Dulbecco's Modified Eagle's Medium (DMEM, high glucose, Gibco™), fetal bovine serum advanced, heat-inactivated (FBS, Capricorn Scientific GmbH), L-glutamine 200 mM solution (Multicell, Wisent Inc.), penicillin–streptomycin solution (10,000 U/mL, Multicell, Wisent Inc.), trypsin EDTA (0.25 % trypsin in HBSS, Multicell, Wisent Inc.) trypan blue solution (0.4 %, Sigma), 7-hydroxy-3H-phenoxazin-3-one-10-oxide sodium salt (Resazurin Sodium Salt, Sigma Aldrich) used as received. All other reagents were purchased from Sigma-Aldrich and were used as received without further purification.

2.2. Characterization

^{1}H (500 MHz) spectra were recorded in $CDCl_3$ with $Si(CH_3)_4$ as the internal standard, using an Agilent VNMRS 500 MHz instrument. The particle size and zeta potential of the PAMP-rGO derivatives were determined in distilled water by dynamic light scattering (DLS) using a Malvern Zetasizer Nano ZSP instrument. UV–Vis and fluorescent measurements of 96-well plates were recorded using the SpectraMax® i3 multi-mode platform, Fourier transforms infrared (FTIR) spectra were recorded on an Agilent Technologies Cary 630 FTIR instrument that is equipped with attenuated total reflectance (ATR), over the range 4000–400 cm^{-1}. Renishaw inVia™ Raman microscope was used for Raman spectroscopy analysis. Transmission and scanning electron microscopy (TEM and SEM, respectively) scans were conducted using a field-emission scanning electron microscope (FE-SEM Zeiss Gemini 500) equipped with an EDX detector. The nanoplatforms were dispersed in water applied on Formvar-coated 200 square mesh nickel grids by drop-casting for TEM scans, where the samples were mounted on double adhesive carbon-coated tape on aluminum stubs for SEM and elemental analyses. Thermogravimetric analyses (TGA) were performed using a TGA 8000 instrument (Perkin Elmer) under a N_2 atmosphere at a heating rate of 10 °C/minute heating rate, between 30–800 °C. Zeiss LSM 800 multiphoton confocal microscope was used for the fluorescence imaging. Dox fluorescence intensity for 50,000 events from Dox and Dox-carrying nanoplatforms treated cells were recorded with BD Biosciences BD Influx™ cell sorter.

2.3. Synthesis of poly[(poly(ethylene glycol) methyl ether methacrylate)–co-(3-azido propyl methacrylate)–co-(methyl methacrylate)–co-(1-pyrenemethyl methacrylate)] graft copolymer (P(PEGMA-co-AzPMA-co-MMA-co-PMA), PAMP)

Multiple pyrene, azide, and PEG-containing graft copolymers were synthesized as described in our previous publication [22]. Some molecules such as the azide-functional monomer 3-azido propyl methacrylate and benzyl functional initiator, which was used as a reference signal in ^{1}H NMR analyses, were synthesized prior to copolymerization [25]. Briefly, monomers at different proportions, including poly(ethylene glycol) methyl ether methacrylate (PEGMA, 500 or 2000 Da), methyl methacrylate (MMA), 3-azido propyl methacrylate (AzPMA), and 1-pyrenemethyl methacrylate (PMA), were added to a 10 mL glass reactor and dissolved in toluene, followed by the addition of PMDETA and copper (I) bromide (CuBr). Finally, a benzyl functional ATRP initiator was added to the reaction mixture and the reactor was sealed and immediately frozen in liquid nitrogen. After three freeze–pump–thaw (FPT) cycles, the reaction mixture was placed in an oil bath at 60 °C for 3 h. Upon completion, the catalysts were removed by aluminum oxide filtration, and the polymer solution was concentrated, precipitated in cold diethyl ether, and dried under vacuum at room temperature. The product was characterized using ^{1}H NMR spectroscopy.

2.4. PAMP coating on graphene oxide and in situ reduction (PAMP-rGO)

The aim was to coat graphene with PEG-containing P(PEGMA-*co*-AzPMA-*co*-MMA-*co*-PMA) (PAMP) copolymers through multiple pyrene units based on previously published protocols by Demirel *et al.* [22]. In summary, GO solution (1 eq by weight, 4 mg/mL in H_2O) was transferred to a round-bottomed flask, and PAMP (10 eq by weight) was dissolved in DMF (DMF: water = 1:2 v/v) and added dropwise to the GO solution. 2 h of stirring at room temperature was followed by hydrazine hydrate addition (1 μL/1 mg GO) and the reaction flask was placed in an oil bath at 80 °C and stirred for 24 h [33]. Next, the reaction mixture was centrifuged at 14,000 rpm for 15 min, the supernatant was discarded, and the pellet was redispersed in water and acetone and centrifuged several times to wash out the free copolymer.

2.5. Preparation of EPPT1 targeted PAMP-rGO or PAMP-rGO-Dox by copper catalyzed azide-alkyne cycloaddition (PAMP-rGO-EPPT1 or PAMP-rGO-Dox-EPPT1)

The alkyne-PEG-EPPT1 polymer was conjugated to azide functionalities on the PAMP-rGO or drug-loaded PAMP-rGO-Dox surface using a $CuSO_4$/sodium ascorbate catalyst system in PBS at pH 8. In a general procedure, 8 mg of $(P_{15}A_{10}MP)_{2000}$-rGO (1 eq of $(P_{15}A_{10}MP)_{2000}$, 1.35×10^{-7} mol) or 15.9 mg $(P_{15}A_{10}MP)_{2000}$-rGO-Dox (corresponding to 8 mg of $(P_{15}A_{10}MP)_{2000}$-rGO, 1 eq of $(P_{15}A_{10}MP)_{2000}$, 1.35×10^{-7} mol) dispersed in PBS (pH 8), 1.27 mg alkyne-PEG-EPPT1 (2 eq, 2.69×10^{-7} mol, targeting 2 units of azide group on the copolymer), $33.6x10^{-3}$ mg of $CuSO_4$ (1 eq, 1.35×10^{-7} mol), and $53.3x10^{-3}$ mg of sodium ascorbate (2 eq, 2.69×10^{-7} mol) were transferred into a Schlenk flask containing 7 mL of PBS at pH 8. The flask was subjected to three FPT cycles before stirring the reaction mixture at 35 °C overnight. The reaction mixture was centrifuged and redispersed thrice in PBS (pH 8) and twice in distilled water to remove unreacted conjugates. The final product was then freeze-dried overnight. The amount of peptide conjugated to the PAMP-rGO surface was calculated by determining the unbound peptide in the upper phase using Ellman's assay, which reacts with the −SH groups of the peptide and forms 2-nitro-5-thiobenzoic acid (TNB), which is soluble in water and has an absorption at 412 nm, to provide a quantitative calculation of the amount of unreacted peptide. A calibration curve at various alkyne-PEG-EPPT1 concentrations was prepared according to the manufacturer's protocol (**Figure S3**) and used to determine the remaining EPPT1 after conjugation.

2.6. Capping remaining azide groups with propargyl alcohol (PMP-rGO-EPPT1)

After EPPT1 peptide conjugation, the remaining azide groups were either left or capped with excess propargyl alcohol to obtain a nonionic, hydrophilic group on the coated surface. Briefly, 10 equivalents of propargyl alcohol was used against the remaining 1 equivalent of the azide group on PAMP-rGO-EPPT1. To the solution of propargyl alcohol and PAMP-rGO-EPPT1 in PBS, $CuSO_4$ (10 eq) and sodium ascorbate (20

eq) were added, and the mixture was stirred at 30 °C for 20 h. The resulting PMP-rGO-EPPT1 composition was washed with PBS and dd-water multiple times and freeze-dried overnight.

2.7. Drug loading on PAMP-rGO or PAMP-rGO-EPPT1 or PMP-rGO-EPPT1 (PAMP-rGO-Dox or PAMP-rGO-EPPT1-Dox and PMP-rGO-EPPT1-Dox)

10 mg of PAMP-rGO, or PAMP-rGO-EPPT1, or PMP-rGO-EPPT1 nanoplatforms were dispersed in 9.9 mL of PBS at pH 8 in a round-bottomed flask using an ultrasonic probe sonicator. 10 mg of doxorubicin hydrochloride (Dox) was dissolved in 0.1 mL of DMSO and added dropwise onto nanoplatform dispersant, and the mixture was stirred overnight at 35 °C in the dark. The reaction mixture was centrifuged at 14,000 rpm for 15 min, and the supernatant was collected to measure the amount of unloaded Dox based on a calibration curve prepared using various concentrations of Dox in PBS (pH 8) containing 10 % DMSO (**Figure S4**). The pellet was washed multiple times with PBS and dd-water. Dox-loaded compositions were redispersed in dd-water before overnight freeze drying.

UV–visible spectroscopy analysis of the initial supernatant of the Dox loading solutions was performed at 484 nm to indirectly calculate the drug-loading efficiencies (LE) and drug-loading capacities (LC) of the carriers by measuring the concentration of free Dox in the supernatant. Drug-loading efficiencies (**Equation (1)** and drug-loading capacities (**Equation (2)** were indirectly determined by measuring the concentration of free Dox in the upper phase.

$$\mathrm{LE\,(weight\%)} = \frac{\text{Weight of loaded drug}}{\text{Weight of drug in feed}} \times 100 \tag{1}$$

$$\mathrm{LC\,(weight\%)} = \frac{\text{Weight of loaded drug}}{(\text{Weight of loaded drug} + \text{Weight of Nanoplatform})} \times 100 \tag{2}$$

2.8. In-vitro drug release study

The release of Dox from the targeted and non-targeted PEGylated nanoplatforms was assessed in PBS buffer (pH 5.5, pH 7.4) by dialysis. Drug-loaded nanoplatforms containing 1 mg Dox were dispersed in PBS at the desired pH, transferred into a dialysis membrane (3.5 kDa MWCO) and placed in a flask containing 110 mL PBS at 37 °C. At predetermined time intervals, 200 μL samples from the flask were withdrawn for analysis, and their absorbance was measured at 483 nm. All experiments were performed in triplicate, and the mass of the released Dox was calculated using a calibration curve prepared at different concentrations of Dox in PBS (**Figure S4**), followed by the calculation of the released drug percentage based on **Equation (3)**.

$$\%\text{Dox Release} = \frac{\text{Mass of Released Dox}}{\text{Initial Dox Mass}} \text{x}100 \tag{3}$$

2.9. Release kinetics

To study the kinetics and mechanism of Dox release from the targeted and non-targeted PEGylated nanoplatforms, the drug release data were fitted to the standard drug release kinetic models that are commonly utilized to analyze drug release from polymeric systems, such as zero-order, first-order, Higuchi, Weibull, and Korsmeyer-Peppas models described by Equations (4)–(8), respectively. The R^2 value for each model was determined, and in tandem with the literature, the release exponent of the Korsmeyer–Peppas model (n value) was determined to describe the Dox release pattern from the nanoplatforms. The data were processed using Microsoft Excel, and the curves were fitted using GraphPad Prism 9 software [25,34].

$$F = K_o t \tag{4}$$

$$Ln(1-F) = -K_f \times t \tag{5}$$

$$F = K_H . t^{1/2} \tag{6}$$

$$Ln[-Ln(1-F)] = -Lna + b \times Ln(t) \tag{7}$$

$$Ln(F) = Ln(K_{KP}) + n \times Ln(t) \tag{8}$$

2.10. Cell culture procedure

The human breast adenocarcinoma cell line (MCF-7) of epithelial origin was cultivated in modified Dulbecco's Eagle Medium (high-glucose DMEM) fortified with 10 % fetal bovine serum (FBS), 1 % MEM non-essential amino acids, and a combination of penicillin and streptomycin at a concentration of 1 % in T-75 cell culture flasks. Cell culture was maintained under controlled conditions of 37 °C and 5 % CO_2 in a humidity-regulated environment.

2.11. Cell viability analysis using resazurin assay

The cellular viability of various nanocarrier compositions was assessed using a resazurin assay (7-hydroxy-3H-phenoxazin-3-one-10-oxide sodium salt). A total of 10,000 MCF-7 cells were seeded into black wall, clear bottom 96-well plates containing 200 μL of culture medium, and incubated overnight to allow for cell attachment. Subsequently, the cells were treated with different nanoplatforms at various Dox concentrations (2.5, 5, 7.5, and 10 μg/mL) or equivalent PAMP-rGO concentrations for non-Dox-loaded nanoplatforms for 24 h. After incubation, the wells were washed with PBS, and 10 μL of resazurin solution (0.2 mg/mL) was added to 190 μL of culture medium and incubated for an additional 2 h. Cell viability was determined by recording the fluorescence of metabolized resorufin at 590 nm with excitation at 550 nm using a microplate reader. The percentage cell viability was calculated and compared to that of untreated cells, and the background fluorescence was subtracted, as described in **Equation (9)**.

$$\%\,\text{Cell Viability} = \frac{\text{Test Well - Negative Control}}{\text{Positive Control- Negative Control}} \text{x}100 \tag{9}$$

2.12. Flow cytometry (FACS) analysis

The cellular uptake rates of targeted and non-targeted Dox-loaded nanoplatforms were determined using flow cytometry. The analysis was performed without additional staining by relying on the natural fluorescence of the Dox molecule incorporated into the structure. A total of 3×10^5 MCF-7 cells were plated into a 6-well plate in 3 mL of culture medium and incubated for 12 h to allow for attachment to the well surface. The Dox-carrying nanoplatforms were dispersed in PBS, diluted with the culture medium, and transferred onto the cells at a concentration of Dox (10 μg/mL) in 500 μL. After 4 h of incubation, the materials were removed from the wells and washed thrice with PBS, and the cells were detached from the well surface using trypsin/EDTA. The cells were washed with PBS containing 2 % FBS, resuspended in this solution, passed through a 40 μm nylon cell strainer, transferred to analysis tubes, and stored on ice. Using a BD Influx™ Cell Sorter, 50,000 events were recorded based on Dox fluorescence (excitation at 488 nm and emission at 550 nm).

2.13. Confocal microscopy analysis

To evaluate the cellular uptake of the targeted and non-targeted drug-loaded PEGylated rGO nanoplatforms, 25×10^3 MCF-7 cells were seeded into a glass-bottom 24-well plate with 1 mL of full growth

medium and incubated overnight for attachment. The Dox-loaded nanoplatforms were then applied to cells at a concentration of 10 μg/mL for 4 h. After treatment, the wells were thoroughly washed three times with PBS, and 1 μL of Hoechst dye dissolved in 1 mL of medium was applied for 15 min to facilitate nuclear staining. Images were captured using a Zeiss LSM 800 Multi-Photon and Confocal Microscope and subsequently analyzed using Zeiss Zen software.

2.14. Statistical analysis

A two-way analysis of variance (ANOVA) with Tukey's post hoc test was performed to determine the significant differences among the groups using GraphPad Prism software (version 8.02; GraphPad Software Inc.).

3. Results and discussion

3.1. Synthesis of functional copolymer (PAMP)

Graphene derivatives have received considerable attention in the field of drug delivery. However, their toxicity, which is dependent on the dose, shape, and contact time, remains an issue of concern and requires regulation to mitigate cytotoxicity. To overcome this challenge, we have presented a well-established PEGylation method that utilizes a combination of pyrene and PEG brush-containing copolymers to coat the surface of GO while reducing it to rGO, which is a more defect-free derivative with regained graphene properties. The proposed method exhibits numerous advantages, including a high coating efficiency of 71 % and the utilization of the surface area of graphene as opposed to its edges. Furthermore, the copolymer can be modified to facilitate the simultaneous delivery of multiple treatments to the graphene surface. Our recent study demonstrated that PEGylated biocompatible rGO-based nanoplatforms can be decorated with targeting peptides and cationic copolymers as gene delivery vehicles by leveraging the functional copolymer used for PEGylation, namely poly[poly(ethylene glycol) methyl ether methacrylate)–*co*-(3-azidopropyl methacrylate)–*co*-(methyl methacrylate)–*co*-(1-pyrenemethyl methacrylate)] (P(PEGMA-*co*-AzPMA-*co*-MMA-*co*-PMA)). This azide-containing copolymer can be functionalized before or after coating on the surface and can be used as a functionalization tool. One of the outcomes of this study was that the positively charged cationic copolymer enhanced drug release compared to the rGO-based system that did not contain the cationic copolymer [25]. This urges the need to investigate the effect of ionic groups on drug release behavior and whether they can be used as both release enhancers and functionalization tools. Moreover, the PEG chains have two different chain lengths and can be used to tune the PEG density at the surface, depending on the number of brushes. Their length and density may also influence their release behavior. To address all these hypotheses, P(PEGMA-*co*-AzPMA-*co*-MMA-*co*-PMA) copolymers were synthesized with different numbers of azide groups along with different lengths and numbers of PEG brushes to examine the effect on release behavior from the surface of rGO (Table 1). Here, two different chain lengths of 500 and 2000 Da for PEGMA were used to tune the PEG content at the surface without drastically increasing the molecular weight of the copolymer and to contribute to the solubility and biocompatibility of the final nanoplatform. As emphasized previously, the PMA monomer provides π-π interactions, whereas MMA allows us to extend the chain. Different numbers of azide groups were introduced to the copolymer using the AzPMA monomer for further functionalization through the "click" reaction and the drug release enhancer through ionic interactions or changing the hydrophilicity of the surface.

As shown in Table 1, P(PEGMA-*co*-AzPMA-*co*-MMA-*co*-PMA) (PAMP) containing PEG brushes, azide, and pyrene groups with different compositions were synthesized via ATRP using benzyl group containing initiator for ease of calculation of required parameter with different feeding ratios to tune the desired copolymer composition (**Scheme S1a**) [25]. Molecular weights and copolymer composition were calculated using ^{1}H NMR spectroscopy (**Figure S1**). It should be noted that controlled polymerization allows us to tune the chain length and monomer composition. PAMP copolymers were designed to contain increasing PEG brush and azide numbers for both compositions with different PEG brush lengths. The overall molecular weight was increased while maintaining consistent composition and pyrene unit numbers, especially for PEG_{2000} composition.

3.2. Preparation of targeted, drug loaded rGO nanoplatforms

Synthesized PAMP copolymers systematically coated on GO surface via π-π interaction through pyrene units. The comparable rGO surfaces were prepared to investigate three main objectives such as the effect of the presence or the number of azide groups on drug release, the effect of the length and density of PEG brushes on drug release, and the effect of the conjugation order of targeting agent or the order between drug loading and targeting agent on release profiles. First, different numbers of azide groups-containing PAMP copolymers were coated on rGO, and to solely see the azide group contribution, azide groups were capped with propargyl alcohol (PMP-rGO) after PAMP coating on the GO surface to mask the charge contribution of the azide group on the carrier while keeping the character hydrophilic. This process was applied to all PAMP-coated surfaces regardless of different PEG chain lengths and the number of brushes, allowing the comparison of the surface with different PEG density with or without azide groups. Next, we sought to investigate the order of targeting agent conjugation and drug loading, as the conjugation of the EPPT1 peptide with the PEG chain may act as an additional diffusion barrier, slowing down the release of the drug. For this purpose, either Dox loading followed by EPPT1 peptide conjugation or first EPPT1 peptide conjugated followed by Dox loading. In both scenarios, the remaining azide groups were capped for each composition to have a better comparison. Fig. 1 shows the preparation of PAMP and PMP-coated, targeted, and non-targeted Dox-loaded rGO surfaces as targeted drug-loaded nanoplatforms. The initial coating on the GO surface was conducted through the interaction of PAMP copolymers and GO in a DMF-water mixture, followed by the chemical reduction of GO to rGO using hydrazine hydrate as a reducing agent. The product was purified by centrifugation and washing with water and acetone to remove unbonded copolymers and hydrazine. As summarized in

Table 1
Features of PAMP copolymers with different compositions.

	Copolymer Code[a]	M_{nNMR}[b] (g/mol)	DP_n	% PEG Density[c]	# of PEGMA	# of AzPMA	# of MMA	# of PMA
PEG_{500}	$(P_{17}A_9MP)_{500}$	15,450	60	55	17	9	24	10
	$(P_{26}A_{16}MP)_{500}$	20,350	65	64	26	16	12	11
PEG_{2000}	$(P_{15}A_{10}MP)_{2000}$	35,500	47	84	15	10	11	12
	$(P_{25}A_{17}MP)_{2000}$	61,500	109	81	25	17	57	11

[a] Monomers/PMDETA/CuBr/Initiator:100/1/1/1. The reaction volume was set to 15 mL by adding toluene. Polymerization proceeded for 3 h, except for the $(P_{15}A_{10}MP)_{2000}$ composition, which proceeded for 5 h.
[b] The M_{nNMR} and monomer ratios were calculated using ^{1}H NMR.
[c] Weight % PEG in the copolymer.

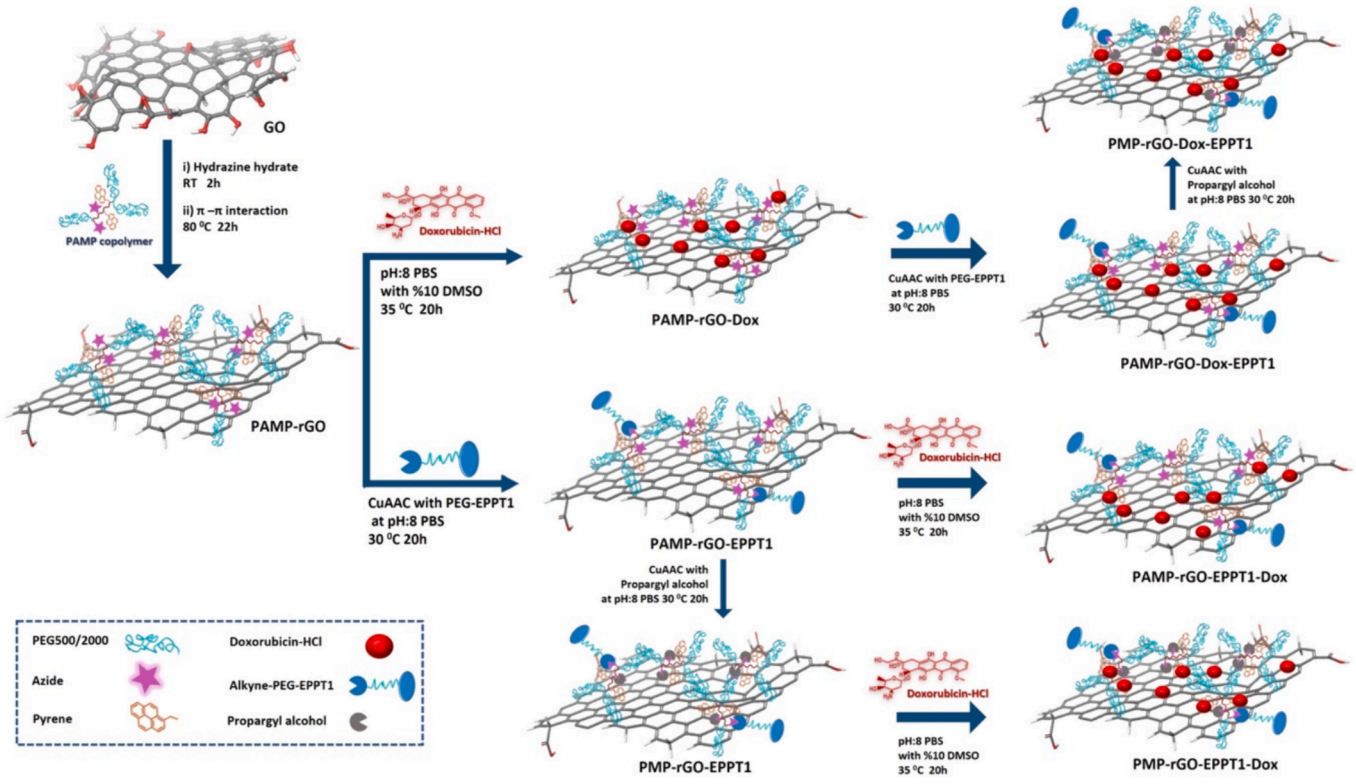

Fig. 1. Preparation paths of various targeted, drug-loaded rGO nanoplatforms.

Table S1, coating efficiencies were once again obtained higher than 60 %, indicating the efficiency of the PEGylation method.

As stated before, the azide functionality in the copolymer was mainly designed and used as a tool for further functionalization. However, it would be beneficial if this functionalization tool could be naturally used as a release enhancer. To address this hypothesis, the effect of azide groups on the carrier's activity was investigated for the first time in the literature. Therefore, GO was coated with azide containing PAMP copolymers and reduced to rGO, then either first Dox loaded followed by EPPT1 peptide conjugation or peptide conjugated followed by Dox loading. The number of azide groups was adjusted to be almost equal to 9 and 16 for PEG_{500} and 10 and 17 for PEG_{2000} to see the effect of increasing azide groups for the same and different PEG brush lengths. Since only some of the azide groups are used in targeting agent conjugation, the remaining azide groups were capped with propargyl alcohol in an aqueous environment using $CuSO_4$ and sodium ascorbate once all the functionalization steps were completed. The disappearance of the azide signal in the FTIR spectrum confirmed the successful reaction between azide and propargyl alcohol. As seen in Figure S2, free AzPMA containing PAMP copolymer and PAMP-rGO clearly showed a stretching band at 2100 cm^{-1}, characteristic of the azide groups, at the same region with the monomer while the azide stretching disappeared for PMP-rGO derivatives, indicating the effective reaction with propargyl alcohol.

To complete the synthesis of the targeted rGO-based nanoplatform, EPPT1, a synthetic peptide used as a targeting peptide against underglycosylated MUC1 (uMUC-1) receptors overexpressed on the membrane surface of metastatic breast cancer cells [35], was conjugated on the prepared rGO surfaces. EPPT1 peptide containing PEG chain was prepared based on previously published work [25] and conjugated on the surface of PAMP-rGO through a "click" reaction using azide groups present on the surface. The conjugation efficiency of the peptide on the surface was determined by the peptide concentration in the upper phase of the centrifuge reaction mixture using Ellman's assay to determine the concentration of EPPT1 peptide through −SH containing cysteine amino acid that EPPT1 peptide contains. The results showed that regardless of coated copolymer compositions, peptide conjugation took place with high reaction yield, and only less than 1 % (weight) peptide did not react and stay in the upper phase (Table S2). Even though "click" reactions are highly efficient reactions, the almost quantitative reaction yield on the surface indicated the possibility of physical interaction between peptide and rGO surface, which is well known in the literature [36].

Finally, Dox, as an anticancer agent, was loaded onto the prepared surface via π-π and hydrophobic interaction before peptide conjugation (PAMP-rGO-Dox-EPPT1) or as the final step (PAMP-rGO-EPPT1-Dox). Similarly, the remaining azide groups were capped after peptide conjugation for both strategies to obtain PMP-rGO-Dox-EPPT1 or PMP-rGO-EPPT1-Dox. Knowing the amount of the loaded drug on the carrier is a significant advantage in tuning the different components comparably during the investigation of the drug release profile. When Dox loading was performed as the last step, the amount of loaded Dox can be easily calculated using the remaining Dox concentration in the supernatant, making this step more favorable for the study. However, it is also possible to load Dox right after PAMP coating to have non-targeted PAMP-rGO-Dox and follow with EPPT1 conjugation as the last step (PAMP-rGO-Dox-EPPT1). This way, the effect of a different drug loading order or peptide conjugation on the drug release profile could be investigated. Regardless of the order of Dox loading, the loaded amount of Dox was calculated using the calibration curve with the linear curve fitting with an R^2 value of 99.8 % (Figure S4). Accordingly, Dox was able to be loaded on copolymer-coated and peptide-conjugated rGO nanoplatforms with a drug loading efficiency range of 92 % to 98 % by weight. Calculated results clearly showed that the length of the PEG brush did not affect the loading efficiency. On the other hand, the temperature of the experiment clearly influenced drug loading efficiency (Figure S5). Drug loading efficiency reached 98.86 % at 35 °C using 10 % DMSO-containing PBS solution, while only 74.8 % under the same conditions at 19 °C.

3.3. Characterization of targeted, drug loaded rGO nanoplatforms

Detailed characterization for different rGO surfaces was carried out before comparing their drug release profile and in vitro anticancer activities. The coating percentage and weight loss behavior differences were investigated using TGA [22]. All compositions are typically analyzed between 30 to 800 °C by heating 10 °C/min under a nitrogen atmosphere. Weight loss associated with PAMP copolymer degradation was used to calculate the copolymer coating efficiency on the graphene surface, considering the contribution of rGO and the weight lost within the same temperature range (200–550 °C); it was calculated only as 8.6 %. Simply, PEGylation was calculated by extracting this value, the amount of rGO, from the mass reduction PAMP-rGO compounds between 200–550 °C. Fig. 2 shows all the compositions for PEG_{500} (Fig. 2**a**) and PEG_{2000} (Fig. 2**b**) cases for azide functional copolymer compositions. Based on the results summarized in **Table S1**, the coating efficiency of PAMP copolymer on the rGO surface was obtained between 59.9 % and 63.7 %, indicating that the copolymer composition does not have a significant effect on coating efficiency. TGA also proves the presence of Dox and EPPT1 in the structure by showing their characteristic weight loss profile; Dox, in particular, displayed a characteristic degradation profile. Even though the presence of the Dox was clearly demonstrated through its characteristic degradation range, the mass of Dox on the carrier could not be calculated using the obtained thermogram since Dox degradation between 200 and 430 °C overlapped with the degradation of the rGO. Moreover, the thermal decomposition of PAMP-rGO-Dox-EPPT1 showed an extra decay in the range of 460 °C to 485 °C which indicated the additional EPPT1 molecules on the compound. Although this decay is only 1.34 %, it can be interpreted as the contribution of the peptide.

SEM was used to visualize the morphological changes in different compositions as well as elemental mapping on the surface of rGO using EDX analysis. Fig. 3 shows the SEM image of PAMP-rGO-Dox, PAMP-rGO-EPPT1-Dox, and the morphological change of their precursors through surface modifications. Microscope images clearly showed the morphological changes that took place with coating and simultaneous reduction. Separated GO flakes become more compact after reduction, and each coated layer changes the surface roughness. Moreover, EDX analysis supported surface functionalization through its % element distribution (Table 2). Before GO was reduced, it consisted of some functional groups, such as carboxyl, hydroxyl, and epoxy groups, contributing to the oxygen percentages (37.97 %). When reduced without any copolymer coating, a significant decrease in the percentage of oxygen (11.28 %) occurred, while a noticeable amount of nitrogen was detected because of trapping hydrazine between the insoluble, stacked graphene layers, which is not a concern for copolymer coated graphene layer with enhancing solubility and dispersibility. When nitrogen-containing $(P_{15}A_{10}MP)_{2000}$ copolymer was coated on the rGO surface, carbon, oxygen, and nitrogen atomic percentages were detected as 68.88 %, 29.72 %, and 1.37 %, respectively. Dox loaded version of the same derivative showed an increase in nitrogen content to 2.09 %, indicating the presence of Dox on the carrier. At the last step, successful conjugation of EPPT1 along with Dox loading even further increased the nitrogen percentage (2.94 %) owing to the amino groups of the amino acids.

TEM was used as another imaging technique to visualize the functional graphene layers by drop-casting them on grids at a low concentration in water and drying them under a vacuum at room temperature. PAMP-rGO-Dox and PAMP-rGO-EPPT1-Dox showed similar morphological views, with the black dots dominantly coming from the reprecipitation of Dox molecules during sample preparation (**Figure S6a and d).** The images supported the presence of the EPPT1 peptide on the PAMP-rGO surface through the morphological change in the images after EPPT1 was conjugated in the final step, which provided better dispersion properties (**Figure S6b and c).** Furthermore, Raman spectroscopy, one of the specific characterization techniques, was used to confirm the reduction, copolymer coating, and Dox loading. The characteristic shifts in D and G bands for each stage are shown in **Figure S7**. GO commonly displays characteristic D and G bands, which indicates the change of electronic configuration on the carbon lattice. D band is associated with the sp^3 hybridization of carbon atoms, and the G band originates from sp^2 carbon atoms vibrations on the plane. The reduction of GO to rGO changes the degree of in-plane defects and functionalities on the surface, resulting in a change in the ratio of D and G band

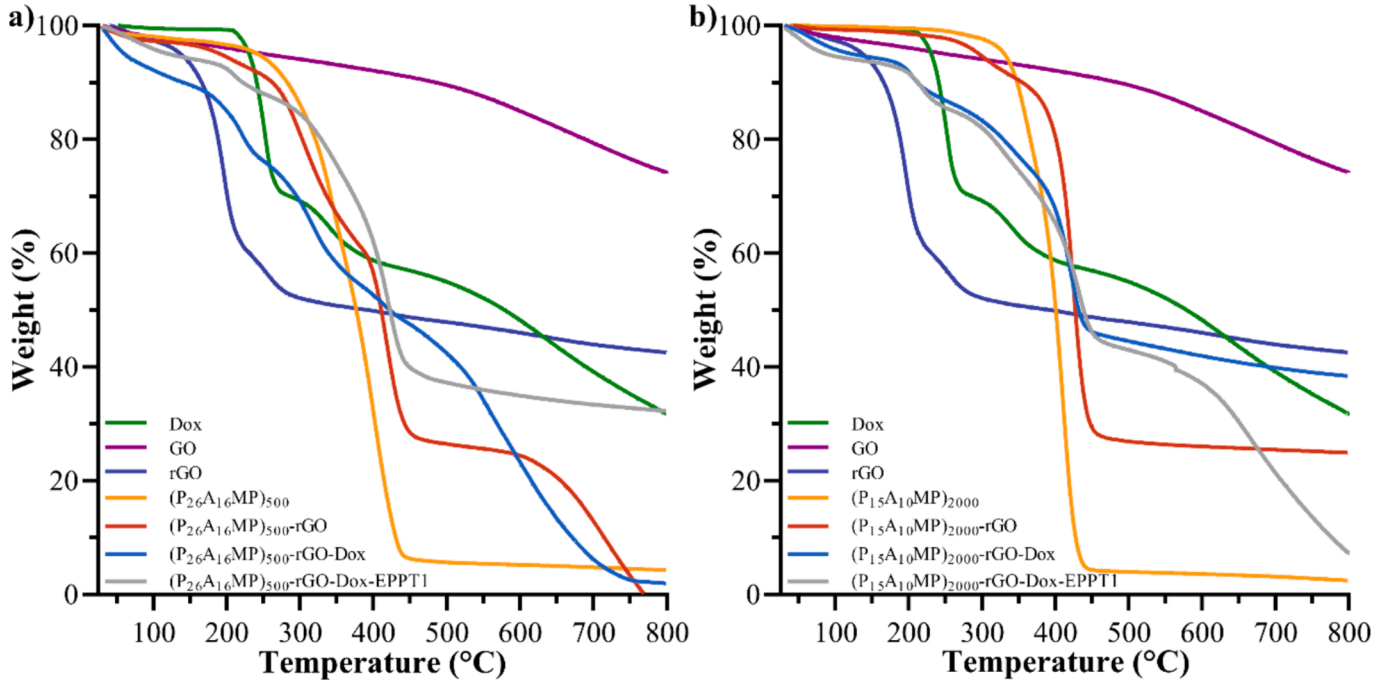

Fig. 2. TGA curves of **a)** GO, rGO, Dox, $(P_{26}A_{16}MP)_{500}$, $(P_{26}A_{16}MP)_{500}$-rGO, and $(P_{26}A_{16}MP)_{500}$-rGO-Dox, $(P_{26}A_{16}MP)_{500}$-rGO-Dox-EPPT1 **b)** GO, rGO, Dox, $(P_{15}A_{10}MP)_{2000}$, $(P_{15}A_{10}MP)_{2000}$-rGO, $(P_{15}A_{10}MP)_{2000}$-rGO-Dox, $(P_{15}A_{10}MP)_{2000}$-rGO-Dox-EPPT1 compounds.

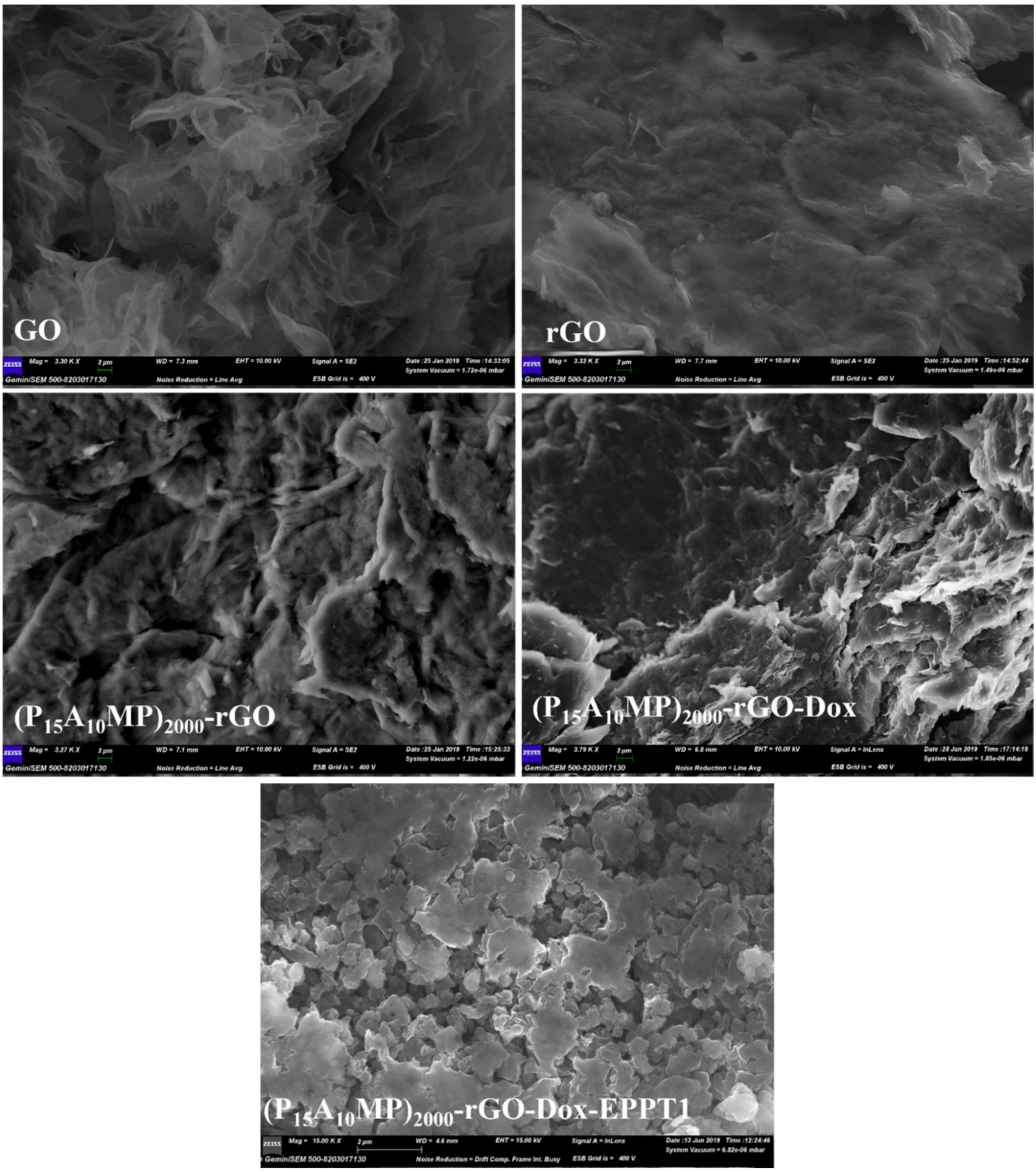

Fig. 3. SEM images of GO, rGO, $(P_{15}A_{10}MP)_{2000}$-rGO, $(P_{15}A_{10}MP)_{2000}$-rGO-Dox, and $(P_{15}A_{10}MP)_{2000}$-rGO-Dox-EPPT1.

intensity [37]. GO showed D and G bands at 1319 cm^{-1} and 1586 cm^{-1}, respectively, and the G band shifted to 1588 cm^{-1} when GO was reduced to rGO, causing a slight decrease in I_D/I_G ratio from 1.31 to 1.29. After PAMP coating and simultaneous reduction, the D band shifted downward to 1313 cm^{-1}, and the G band shifted upward to 1596 cm^{1}, resulting in a narrower G band. The decreased I_D/I_G ratio increased when GO was coated and simultaneously reduced, which indicates the interaction between the copolymer and the graphene surface. Since Dox loading increases this interaction even further, a decrease in I_D/I_G ratio was observed even more significantly, from 1.25 to 1.05, after Dox loading on the PAMP-rGO surface.

The size and surface charge of the rGO-based nanoplatforms obtained through different orders of coating and drug loading were measured using DLS. Our previous work showed that the composition with higher percent PEG density had better dispersion properties and better culture medium stability [22]. Due to this reason, two

Table 2
Elemental analysis results obtained by SEM-EDX analysis.

Compound	C%	O%	N%
GO	59.51	37.97	0.59
rGO	85.99	11.28	2.60
Dox	57.37	33.25	5.06
$(P_{15}A_{10}MP)_{2000}$-rGO	68.88	29.72	1.37
$(P_{15}A_{10}MP)_{2000}$-rGO-Dox	66.26	31.46	2.09
$(P_{15}A_{10}MP)_{2000}$-rGO-Dox-EPPT1	64.07	32.99	2.94

compositions that had the highest PEG density with all possible coating and drug loading orders were selected and their data were presented in Fig. 4. The results indicated that final compositions containing 2000 Da PEG brushes resulted in a smaller size than 500 Da PEG-containing compositions, meaning that longer PEG brushes indicate better dispersion properties. The percentage of PEG density was calculated as 85 % and 64 % for PEG_{2000} and PEG_{500} containing PAMP copolymer, respectively. These values slightly increase with the addition of EPPT1 peptide since it has a 3500 Da length PEG chain. This contribution was more evident for PEG_{500} derivatives, which showed better dispersion and smaller size values after EPPT1 conjugation (306 nm), while the EPPT-free Dox-loaded composition, $(P_{26}A_{16}MP)_{500}$-rGO-Dox, showed the biggest size of 580 nm. Conversely, although azide groups are ionic, they did not enhance the dispersion properties at the end of the propyl chain. For instance, $(P_{15}MP)_{2000}$-rGO-EPPT1-Dox, in which all the azide groups were capped with propargyl alcohol, had a size of 274 nm compared to 364 nm of its azide-containing analog, $(P_{15}A_{10}MP)_{2000}$-rGO-EPPT1-Dox. Notably, this effect most likely plays a role in dispersion properties on PEG_{500} derivatives along with the percentage of PEG density. Moreover, all final compositions with peptide and drug on the surface resulted in a size smaller than 350 nm, which is acceptable for a rGO-based system. It is important to note that measuring the size of the graphene-based drug delivery system has its own challenges because of the 2D graphene sheets. As PEGylated rGO nanoplatform, almost all carriers exhibited negative surface charge, which varied depending on the incorporated components. Negatively charged PEG-containing copolymer-coated and peptide-conjugated Dox-free composition PAMP-rGO-EPPT1 showed the highest negative surface charge of –32.8 mV. Once Dox is loaded, the negative charge decreases to −3.63 mV, as expected, supporting the presence of the drug on the surface. The comparison of azide-containing ($(P_{15}A_{10}MP)_{2000}$-rGO-EPPT1-Dox) and azide-capped analog ($(P_{15}MP\text{-rGO})_{2000}$-EPPT1-Dox) showed a slightly negative surface charge contribution of the azide group. A positive charge of 17.3 mV was only observed for Dox loaded $(P_{26}A_{16}MP)_{500}$-rGO-Dox due to the low PEG content along with the presence of Dox.

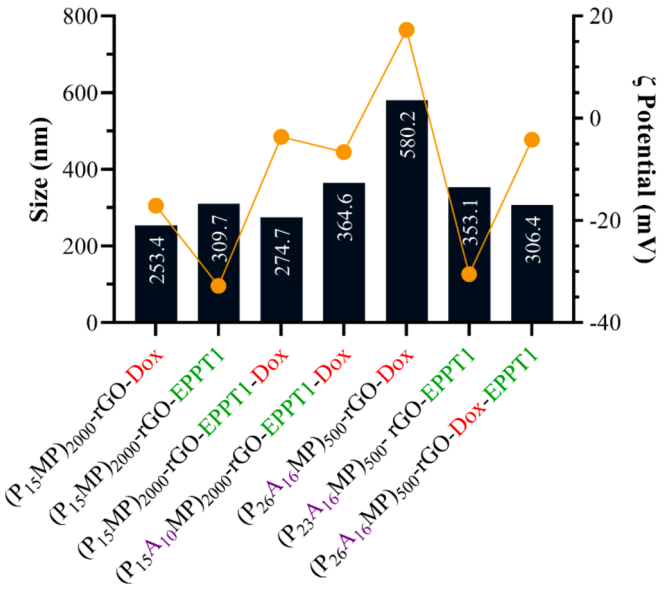

Fig. 4. Size and zeta (ζ) potential analysis of targeted drug-loaded rGO nanoplatforms.

3.4. Investigation of drug release profile of targeted drug loaded rGO nanoplatforms

Even though rGO has restored graphene properties and might be preferred for some biological applications, its drug release activity is limited due to the tighter interaction between the surface and the drug, especially for the drug-loaded ones, through π-π interaction. Therefore, it might be seen using external stimuli to enhance drug release [38,39]. Since graphene derivatives used for biological applications carry surface decoration, it can be useful to know the contribution of the decoration on drug release to tune the release or select the right sequence for conjugation. The contribution of PEG chain length, azide groups, and the order of targeting agent conjugation on drug release were systematically investigated to explore this detail for the previously optimized PEGylation method. In addition to knowing the chain length contribution or whether the targeted agent is supposed to be conjugated before or after drug loading, knowing whether azide groups that were initially designed for the functionalization tool have a role as release enhancer might be a practical strategy that provides more advantages than its intended usage. First, to address whether the presence of azide groups influences Dox release, Dox was loaded on the PAMP-rGO for both PEG chain lengths. Then, intentionally, all azide groups were capped with propargyl alcohol to obtain PMP-rGO derivatives without free azide groups. Once the release profile of PAMP-rGO-Dox and PMP-rGO-Dox were compared, different behaviors were observed for PEG_{500} and PEG_{2000} derivatives, showing the effect of PEG density of the rGO surface (Fig. 5). Fig. 5**a** shows that the azide group contribution to drug release becomes more significant when the carrier has shorter but denser PEG brushes. For instance, $(P_{17}MP)_{500}$-rGO-Dox released more Dox than $(P_{17}A_9MP)_{500}$-rGO-Dox with a PEG density of 55 %, however, $(P_{26}MP)_{500}$-rGO-Dox with the 64 % PEG density released less Dox than its azide containing $(P_{26}A_{16}MP)_{500}$-rGO-Dox analogue. The less dense, short PEG chains do not have any influence on the drug release as they are not dense enough to create a diffusion barrier to slow down the release. This is most likely the Dox release from rGO surface that is independent than copolymer and its composition. That is why it reaches up to maximum release (49 %) among all derivatives. The effect of PEG chain density can only become dominant if they are denser on the surface with an increasing number of brushes for PEG_{500}. This data is consistent with the literature. It was computationally shown that 500 Da PEG chains are folded on the GO surface [31]. If they are dense enough, they can cover more area and have an effect on Dox release from the rGO surface. This might be the reason for more short brush containing $(P_{26}MP)_{500}$-rGO-Dox having slower Dox release. Additionally, 16 of the azide groups were capped with propargyl alcohol which might contribute to some additional hydrogenbonding with Dox or might change the hydrophilicity of the surface. As for longer PEG brushes, the azide group effect is more visible for a smaller number of brushes containing copolymer-coated derivatives ($(P_{15}A_{10}MP)_{2000}$-rGO-Dox vs $(P_{15}MP)_{2000}$-rGO-Dox) than the higher number of brushes containing copolymer-coated derivatives ($(P_{25}A_{17}MP)_{2000}$-rGO-Dox vs $P_{25}MP)_{2000}$-rGO-Dox) (Fig. 5**b**). 15 PEG_{2000}-containing copolymer with 10 azide groups released more drug (37 %) than its azide-capped derivative (28 %); however, when the brush number increased to 25 along with azide number (17), the drug release of azide-containing derivative did not increase, indicating that the azide groups are not the only thing affecting the release; an increasing number of long brushes has more influence on the release behavior. $(P_{25}MP)_{2000}$-rGO-Dox derivative exhibited the maximum release as 44 % for the PEG_{2000} series, especially after 36 h, indicating dominant PEG contribution on the release. It has been shown that longer PEG chain on graphene surface creats dense hydrated layer

a)

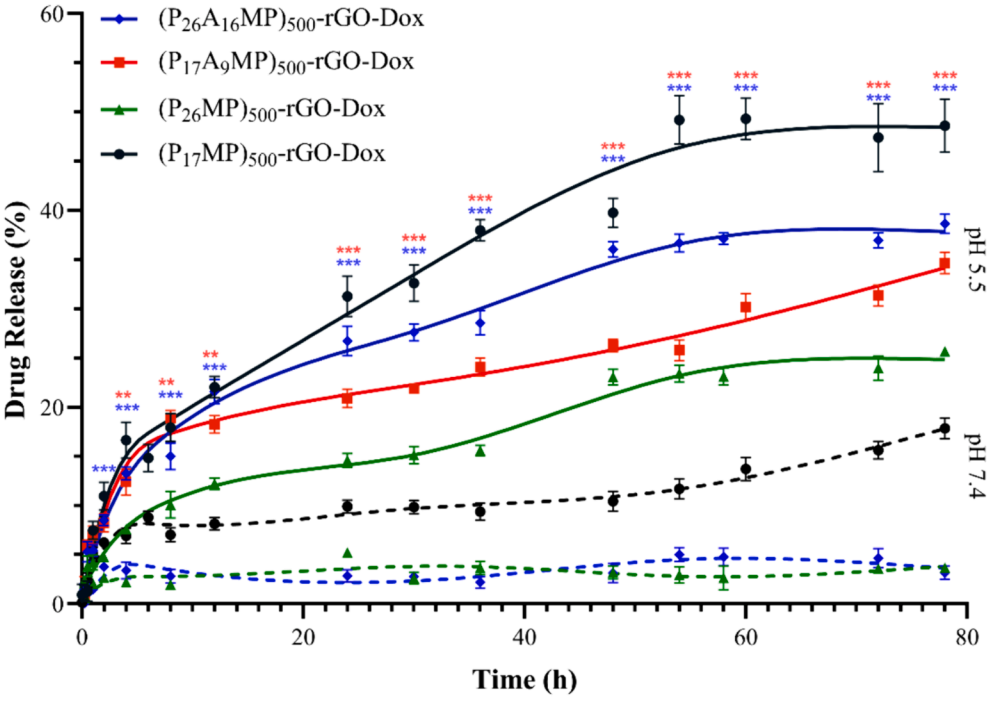

b)

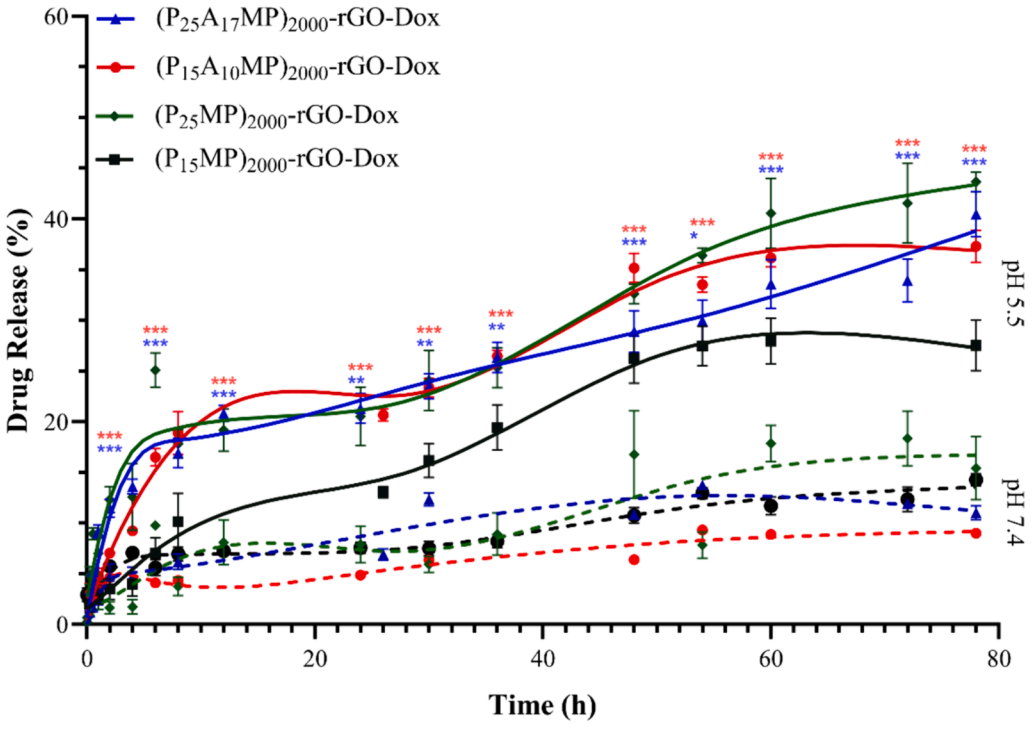

Fig. 5. Cumulative drug release profile of **a)** $(P_{17}A_9MP)_{500}$-rGO-Dox, $(P_{26}A_{16}MP)_{500}$-rGO-Dox, $(P_{17}MP)_{500}$-rGO-Dox and $(P_{26}MP)_{500}$-rGO-Dox at pH 5.5 and 7.4. The plotted values represent the mean ± SEM of three independent experiments. *Significance levels were assigned as* $p < 0.033$ (*), $p < 0.002$ (**), and $p < 0.001$ (***). *Red *** indicates* $(P_{17}A_9MP)_{500}$*-rGO-Dox* vs $(P_{17}MP)_{500}$*-rGO-Dox and blue *** indicates* $(P_{26}A_{16}MP)_{500}$*-rGO-Dox* vs $(P_{26}MP)_{500}$*-rGO-Dox,* **b)** $(P_{25}A_{17}MP)_{2000}$-rGO-Dox, $(P_{25}MP)_{2000}$-rGO-Dox, $(P_{15}A_{10}MP)_{2000}$-rGO-Dox, $(P_{15}MP)_{2000}$-rGO-Doxat pH 5.5 and 7.4. The plotted values represent the mean ± SEM of three independent experiments. Red **** indicates* $(P_{15}A_{10}MP)_{2000}$*-rGO-Dox* vs $(P_{15}MP)_{2000}$*-rGO-Dox, and blue *** indicates* $(P_{25}A_{17}MP)_{2000}$*-rGO-Dox* vs $(P_{25}MP)_{2000}$*-rGO-Dox.* (For interpretation of the references to colour in this figure legend, the reader is referred to the web version of this article.)

and covers GO surface better, favoring Dox-PEG chain interaction [31]. As such, Dox interacts more with increasing PEG_{2000} chains than the rGO surface since longer PEG brush provides better coverage and denser hydration layer on the surface. Probably, the diffusion-based drug release takes place from the PEG layer.

It should be noted here that exhibited drug release percentages can be considered as an achievement for rGO-based drug delivery systems. Dox mainly interacts with GO through π-π stacking and hydrogen bonding. In our system, GO was chemically reduced to rGO, which has a less functional group for hydrogen bonding. In the acidic environment, hydrogen bonds get weaken, and Dox release accelerates. Due to the interaction type, Dox release can take place more efficiently from the GO surface than the rGO surface. Several examples in the literature using rGO as a graphene-based platform yielded around 30 % cumulative releases over time, indicating that most of the Dox still retains on the rGO surface due to the relatively stronger π-π interaction [40]. Some researchers used external stimuli to increase drug release from the rGO surface, such as laser radiation [41] and the introduction of small molecules to the surface that change the hydrophilicity of the surface [42]. Our results collectively supported this thought as presented in Fig. 5 **a** and **b.** While 16 azide groups-bearing $(P_{26}A_{16}MP)_{500}$-rGO-Dox released 39 % of the Dox, $(P_{26}MP)_{500}$-rGO-Dox, the azide-capped analog, only reached the 26 % drug release rate after 48 h at the pH value of 5.5, indicating the clear contribution of the azide group on release for shorter PEG length which requires certain PEG density (>64 %) to be visible. Similarly, $(P_{15}A_{10}MP)_{2000}$ and $(P_{15}MP)_{2000}$-coated rGO nanocarriers released 37 % and 28 % of the Dox, respectively, under the same conditions as a composition that has the PEG density of 84 %, allowing to observe the azide group effect. When the number of PEG brushes increased to 25 ($(P_{25}A_{17}MP)_{2000}$-rGO-Dox vs $(P_{25}MP)_{2000}$-rGO-Dox) without changing the PEG density significantly (81 %), the azide group effect was diminished by the contribution of the increasing number of PEG brushes which favorited the Dox-PEG chain interaction more than Dox-rGO surface interaction.

Controlled polymerization technique allows us to tune the number of PEG brushes and the azide groups in the copolymer that has the different PEG brush length. This way, it is possible to compare them to assess the effect of the PEG brush length on the drug release. Based on the data presented in Fig. 5 **a and b**, $(P_{17}MP)_{500}$-rGO-Dox and $(P_{15}MP)_{2000}$-rGO-Dox have almost same number of PEG brushes (17 vs 15) but different length showing the Dox release of 49 % and 28 %, respectively. Similarly, $(P_{26}MP)_{500}$-rGO-Dox and $(P_{25}MP)_{2000}$-rGO-Dox are almost having the same (26 vs 25) but higher number of brushes compared to other analogues. Their drug release percentages at acidic environment are 26 % and 44 %. These data indicating that for short and long PEG brush containing composition are not acting similar in terms of Dox interaction and release. These findings can be explained with the different characteristics of PEGylated rGO surface that is coated with short or longer PEG as it is computationally well studied in the literature [31] Mahdavi at al. showed that Dox electrostatically interacts more with PEG chains once GO coated with longer PEG brushes and the Dox and PEG interaction have more contact area than Dox and GO surface interaction. Moreover, PEGylation increases water hydration layer which increases with the increasing PEG brush length. This helps us to explain why drug release % increases for $(P_{15}MP)_{2000}$-rGO-Dox and $(P_{25}MP)_{2000}$-rGO-Dox from 28 % to 44 %. Increasing PEG brush on the surface increases the chance of having more Dox on the PEG layer. This is also consistent with the data showing increase once we have azide group on PEG_{2000} containing copolymer, it shows a noticeable effect for less number of PEG containing derivative since more brushes with more Dox-PEG chain interaction dominates the release behavior. Moreover, the drug release behavior of PEG_{2000} coated rGO derivatives at physiological pH supported the Dox and PEG layer interaction by having relatively higher release at around 15 %. For shorter PEG length, it is expected to have more interaction between Dox and rGO surface. In this case Dox is loaded on the rGO surface and the release from the rGO surface might get influenced by the increasing number of short PEG brushes. Having more short brush might shield the Dox already interacted with rGO surface and slow down its release ($(P_{17}MP)_{500}$-rGO-Dox vs $(P_{26}MP)_{500}$-rGO-Dox). It should be noted here that PEG_{500} coated rGO nanoplatform has a heterogeneous nature with more drug aggregation potential and less water dispersibility of the platform. In this study, pyrene groups of copolymers are the main driven force for coating through π-π interaction, however the backbone of the copolymer is expected to be interacted with rGO surface since it is hydrophobic. This provide distributed PEG brushes on the surface while azide groups are closer to the backbone and graphene surface as well. This might be the reason why azide group effect is visible for only a smaller number of longer PEG and higher number of shorter PEG brush since more likely Dox has a chance to locate more closer to the surface.

To gain further information about the release kinetic of the PEGylated rGO surfaces, five well known mathematical models such as zero-order, first order, Higuchi, Weibull, and Korsmeyer-Peppas were employed to all rGO nanoplatforms and their data were analyzed based on the model function in GraphPad Prism by linear regression curve fitting. **Table S3** summarizes the regression modules of each model to determine the most suitable drug release kinetic model (**Figure S8**). The majority of the PEGylated rGO nanoplatform tested in our study show a correlation with either Korsmeyer Peppas or Weibull model indicating the drug release from a polymer or matrix-based system. The R^2 value of Korsmeyer Peppas or Weibull model were close to each other within the range of 0.4951–0.9854. Toylar et al. used the functional graphene-based Dox delivery systems published in the literature and investigated the Dox release kinetics based on known mathematical models [43] and the findings of the study consistent with our data. It was shown that the PEGylated GO systems have good correlation with Weibull model suggesting same drug release mechanism for the different systems, even though pH affects their drug release. This model is commonly used for matrix-based systema for both rapid release and extended drug delivery system [44,45] due to its sensitive parameters and flexibility. The Korsmeyer Peppas model is used for polymeric systems and the value of n defines the two distinct drug release behavior like diffusion or polymer swelling where $n < 0.5$ suggest diffusion control release (Fickian or quasi-Fickian diffusion) and $n = 1$ refers to polymer swelling (case II transport), between these two conditions $0.45 < n < 0.89$ indicates anomalous (non-Fickian) transport [46]. **Table S3** shows that the PEGylated rGO based nanoplatforms that fit with Korsmayer Peppas model had the n value either equal or smaller than 0.5 (except targeted nanoplatforms) indicating the Fickian type drug diffusion mechanism from the surface. PEG_{2000} containing copolymer coated rGO nanoplatform compared to PEG_{500} containing copolymer coated one were more correlated with this model and this might be because of the effect of interaction of Dox and longer PEG chain on release behavior. Even though their R^2 values were high for Korsmeyer-Peppas and Weibull models, $(P_{17}MP)_{500}$-rGO-Dox and $(P_{15}MP)_{2000}$-rGO-Dox nanoplatforms were correlated to Higuchi model at acidic pH. This model describes the diffusion process based on Fick's first law as well [47] There is consistent example showing the Dox release from PEGylated MWCNT surface through diffusion-controlled mechanism by fitting with these two models [20]. When azide containing and capped version of same number of PEG brushes containing compositions were compared, n value of Korsmeyer −Peppas model were close each other even though they have better fit with another model. This might indicate that azide group does not significantly change the mechanism of the drug release which all n were smaller than 0.5 except $(P_{17}MP)_{500}$-rGO-Dox which had the $n = 0.62$ indicating anomalous transport. Zero order model rarely correlates to complex nanocarrier, only $(P_{17}A_9MP)_{500}$-rGO-Dox showed the correlation to zero order at acidic pH might refer to the solubility of the drug on rGO surface.

Targeting agent conjugation after or during PEGylation is one of the most frequently used strategies for targeted drug delivery systems. PAMP-rGO surface is ready for further peptide conjugation because of its

azide groups. Since custom synthesized EPPT1 peptide does not come with an alkyne end group, it was conjugated to alkyne functional PEG to have the reactive site. The conjugation of the EPPT1 peptide on the surface might serve as an additional coating layer or a component that changes the charge and lipophilicity of the surface. Besides the existence of these components on the carrier, the incorporation order of Dox and EPPT1 peptide into the structure might affect the performance of the carrier. Because of these reasons, all these parameters and their synthetic order were investigated in terms of whether they affect the release behavior of the rGO nanoplatform where all these components are built. Therefore, the EPPT1 peptide was conjugated onto PAMP coated, Dox-loaded rGO surface through azide groups. The peptide has a lipophilic structure with both hydrophilic and hydrophobic amino acids that can affect the overall hydrophilicity of the coated rGO surface. Even though it is covalently conjugated to the rGO surface, the pending side of the chain can also interact with the rGO surface via a suitable amino acid and act as an additional layer. To investigate the effect of the presence of peptides on the surface, peptide-conjugated and non-conjugated analogous were compared (Fig. 6). The results showed that the presence of the EPPT1 peptide on the surface of coated rGO clearly reduced the drug release. While $(P_{15}A_{10}MP)_{2000}$-rGO-Dox carrier released 35 % of the loaded Dox at a pH of 5.5 within 48 h, $(P_{15}A_{10}MP)_{2000}$-rGO-Dox-EPPT1 carrier released 16 % of the Dox under the same conditions. Similarly, the drug release of the short PEG brush-containing $(P_{26}A_{16}MP)_{500}$-rGO-Dox decreased from 39 % to 31 % when the EPPT1 peptide was conjugated on the surface.

The EPPT1 peptide might act as an additional layer on already loaded Dox on the rGO surface or it might change the level of interaction between Dox and PEG chains due to the additional PEG chains come with peptide and the lipophilic feature of the peptide. On the other hand, the peptide-conjugated surfaces can often increase the hydrogen bonding and allow the drug to be more readily available in case of a pH change. Therefore, the order of EPPT1 conjugation (or order of Dox loading) needed to be investigated as the next step to find whether it affects the release rate. Fig. 7**a** shows that when Dox loading was performed as the last step after EPPT1 conjugation, the release was accelerated compared to EPPT1 conjugation performed after Dox loading, indicating the change on the PEGylated rGO surface by the conjugation of lipophilic peptide. However, this is not valid for azide-capped composition (Fig. 7**b**). In that situation, the order of EPPT1 conjugation was not significant for the initial 48 h, and $(P_{15}MP)_{2000}$-rGO-Dox-EPPT1 accelerated slightly after 60 h. The regression modules of tested release kinetic models for these compositions presented in **Table S3** showed that the release profile of $(P_{15}MP)_{2000}$-rGO-EPPT1-Dox fits better with Higuchi model at acidic pH, while the release profile of $(P_{15}MP)_{2000}$-rGO-Dox-EPPT1 shows superior fit with first order. The obtained n value (0.95) using Korsmeyer Peppas model for this composition indicated the polymer swelling based drug release that might be related to the change in the surface hydrophilicity. Similarly, the order of EPPT1 peptide conjugation and Dox loading was further investigated for shorter PEG_{500} brush-containing compositions. The results showed that the order of Dox loading did not change the drug

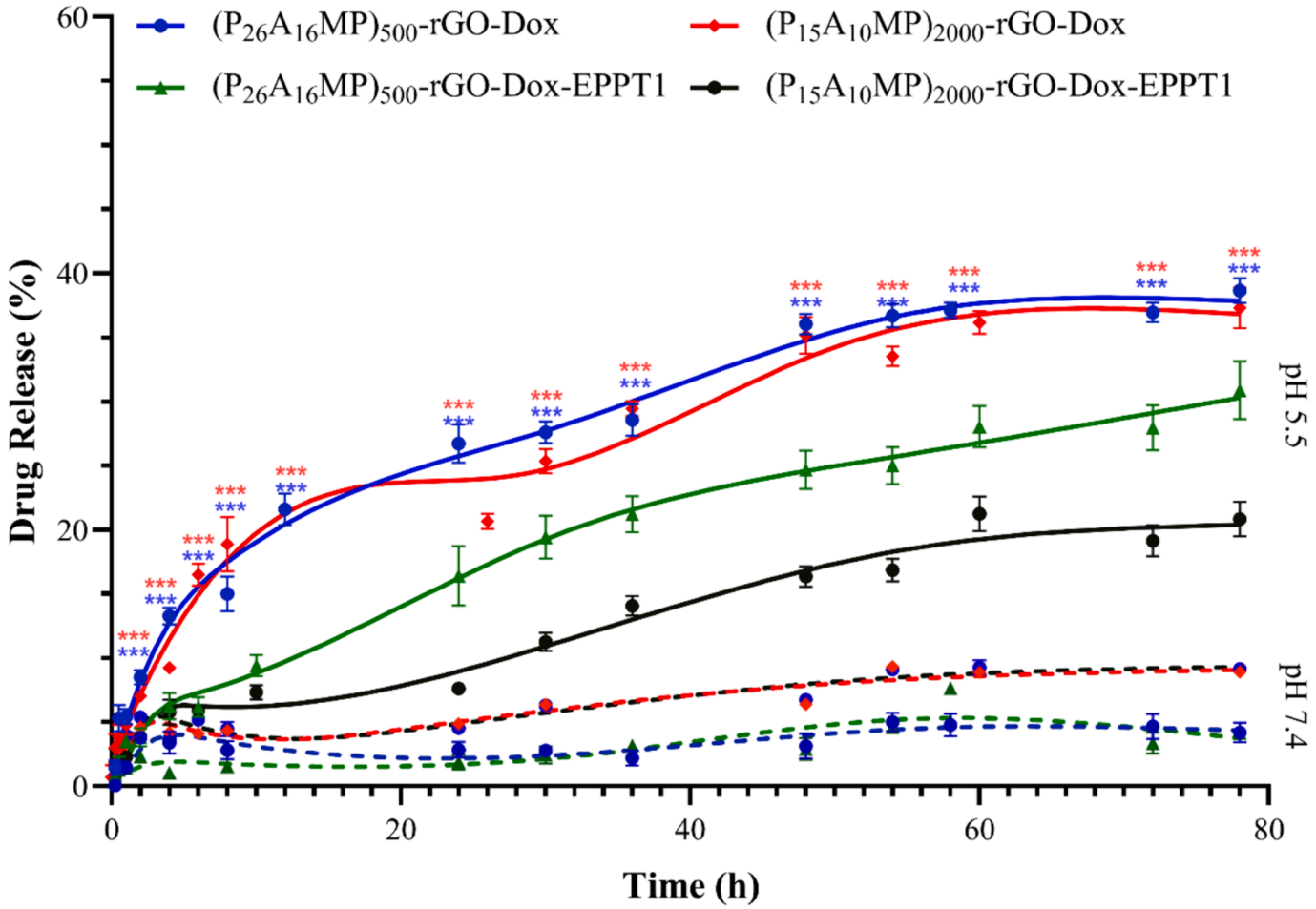

Fig. 6. Cumulative drug release profiles of the $(P_{26}A_{16}MP)_{500}$-rGO-Dox, $(P_{26}A_{16}MP)_{500}$-rGO-Dox-EPPT1, $(P_{15}A_{10}MP)_{2000}$-rGO-Dox and $(P_{15}A_{10}MP)_{2000}$-rGO-Dox-EPPT1 at pH 5.5 and 7.4. The plotted values represent the mean ± SEM of three independent experiments. Significance levels were assigned as $p < 0.033$ (*), $p < 0.002$ (**), and $p < 0.001$ (***). *Blue* *** *indicates* $(P_{26}A_{16}MP)_{500}$-*rGO-Dox* vs $(P_{26}A_{16}MP)_{500}$-*rGO-Dox-EPPT1 and red* *** *indicates* $(P_{15}A_{10}MP)_{2000}$-*rGO-Dox* vs $(P_{15}A_{10}MP)_{2000}$-*rGO-Dox-EPPT1*. (For interpretation of the references to colour in this figure legend, the reader is referred to the web version of this article.)

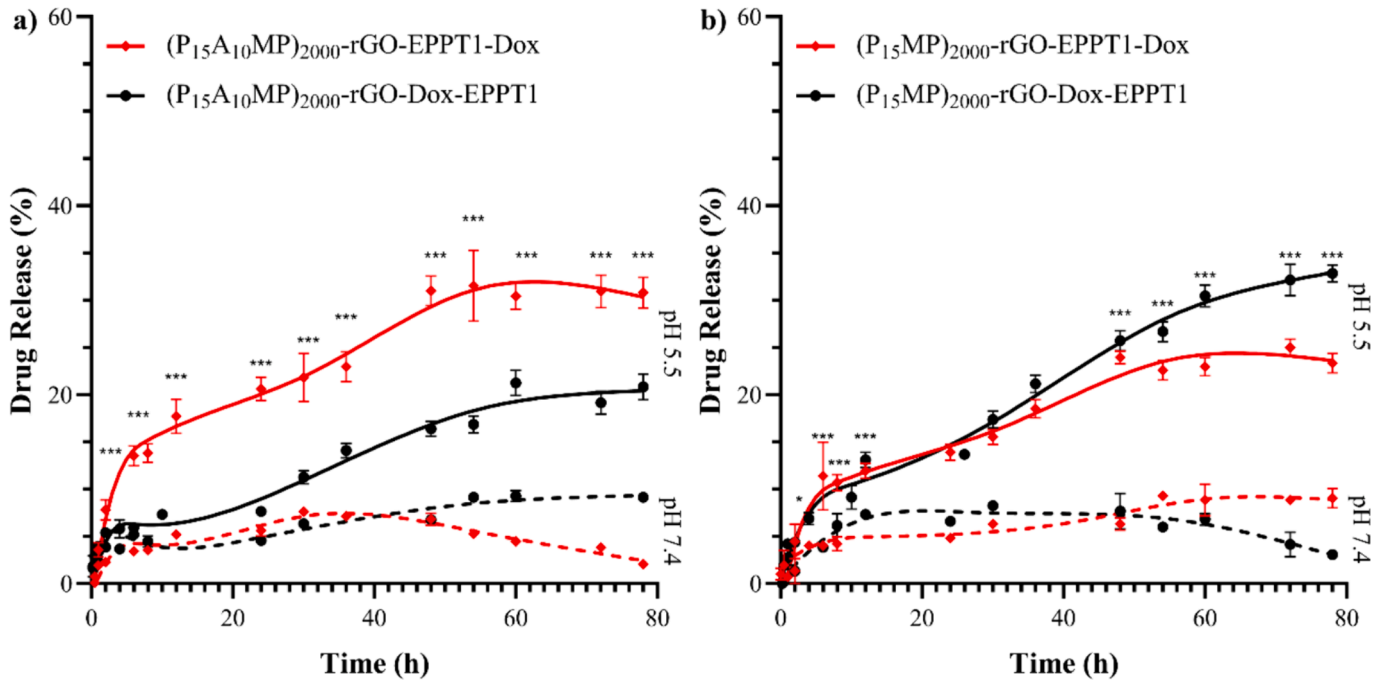

Fig. 7. Cumulative drug release profiles of the **a)** $(P_{15}A_{10}MP)_{2000}$-rGO-EPPT1-Dox and $(P_{15}A_{10}MP)_{2000}$-rGO-Dox-EPPT1 and **b)** $(P_{15}MP)_{2000}$-rGO-EPPT1-Dox and $(P_{15}MP)_{2000}$-rGO-Dox-EPPT1 at pH 7.4 and 5.5. The plotted values represent the mean ± SEM of three independent experiments. Statistical significances are indicated as $p < 0.033$ (*), $p < 0.002$ (**), and $p < 0.001$ (***).

release rate for azide group-containing composition (**Figure S9**). On the other hand, the azide-capped version responded to the order of the Dox loading by slowing down the Dox release when Dox loading was followed by EPPT1 conjugation after 30 h (**Figure S9b**).

Collectively our results showed that when Dox loading was performed as the last step during the preparation of the targeted rGO-based carrier, the drug release profile gave accelerated release. When we compare our results with a similar example in the literature, the components of the proposed PEGylation method naturally enhance the drug release of the rGO-based system. As mentioned before, GO derivatives were preferred more for drug delivery applications because of better water solubility behavior. Yang et al. reported that the drug release percentage of Dox-loaded GO without any surface coating reached 71 % at pH 2, which is the pH that breaks up all the possible hydrogen bonding [48]. Other studies that coated GO surface with Pluronic F127 and PEG exhibited 56 % at pH 5 and 60 % at pH 4.5, respectively [49,50]. Moreover, Depan et al. prepared chitosan-coated GO-bearing folic acid as a targeting agent. They reported that an additional polymer layer slowed down the drug release from 35 % to 24 % compared to the non-coated Dox-GO system at pH 5.3 [51]. Even though all these examples used GO, their results supported that release behavior depended on coating, hydrogen bonding strength, and pH. When rGO is used as a graphene derivative instead of GO, the strength of the hydrogen bonding naturally gets weaker since the number of functional groups decreases with the reduction; however, π-π interaction gets more robust due to the restored graphene surface. In this case, any additional tool that enhances the drug release will be valuable for the application that needs drug release with better graphene properties. In this regard, Cheon et al. used BSA to reduce and coat graphene and loaded Dox as an anticancer agent. The reported drug release was 23 % at pH 5; however, when NIR laser irradiation was applied, drug release rose up to 50 %, indicating the synergetic effect of external stimuli [38]. Herein, our system, just with its PEGylation components, showed the Dox release from the rGO surface within the range of 26–49 %, which can be tuned with the number of azide groups, length of the PEG brush, PEG density, and drug loading order.

3.5. In vitro evaluation of targeted drug loaded rGO based nanoplatforms

The results of detailed drug release studies showed that the targeted platform released more drug when it had azide groups and Dox loading was performed after EPPT1 conjugation for denser PEGylated surface, which showed better biocompatibility based on our previously published study [22]. As a next step, the best composition and their precursors as a control to understand its behavior better were used as a drug carrier to investigate the anticancer activity on breast cancer cells such as the MCF-7 line, which significantly expresses the uMUC1 on the cell surface [52]. To determine the cytotoxicity and biocompatibility of the nanocarriers, free Dox, PAMP-rGO-EPPT1, PMP-rGO-EPPT1 as empty carriers, PAMP-rGO-Dox and PMP-rGO-Dox as non-targeted drug carriers and PAMP-rGO-EPPT1-Dox and PMP-rGO-EPPT1-Dox as targeted drug carriers for both 500 and 2000 Da PEG containing compositions were assessed in the cell viability experiments by resazurin assay for 24 and 48 h of interaction with MCF-7 cancer cell line. Different Dox concentrations such as 2.5, 5, 7.5, and 10 μg/μL were set as the same for all drug carriers, and the same amount of carriers was used for empty carriers to test their effects on cell viability. As can be seen in Fig. 8, the empty carriers ($(P_{15}A_{10}MP)_{2000}$-rGO-EPPT1 and $(P_{15}MP)_{2000}$-rGO-EPPT1) did not show any reduction in cell viability, on the contrary, they showed cell proliferation, indicating the biocompatibility of the carrier [53]. Accelerated release performance of azide-containing non-targeted $(P_{15}A_{10}MP)_{2000}$-rGO-Dox started to show lower cell viability compared to $(P_{15}MP)_{2000}$-rGO-Dox for 48 h incubation, reflecting the release behavior. Even though long-term incubation of cell culture is not ideal for demonstrating the selectivity of the targeting agent, the results obtained for 24 h showed that targeted and Dox-loaded compositions reduced cell viability better than non-targeted analogues (Fig. 8**a**). As was shown in the drug release profile data, EPPT1 targeted carrier with or without azide released more Dox over 48 h which starts showing time and dose-dependent release for 2.5, 5, and 7.5 μg/μL by killing almost 75 % of the cancer cells (Fig. 8**b**). All Dox-loaded targeted compositions showed similar cell viability with the free drug at 7.5 and 10 μg/μL concentration, considering the fact that they are targeted nanocarriers that can accumulate into the tumor through enhanced permeability and

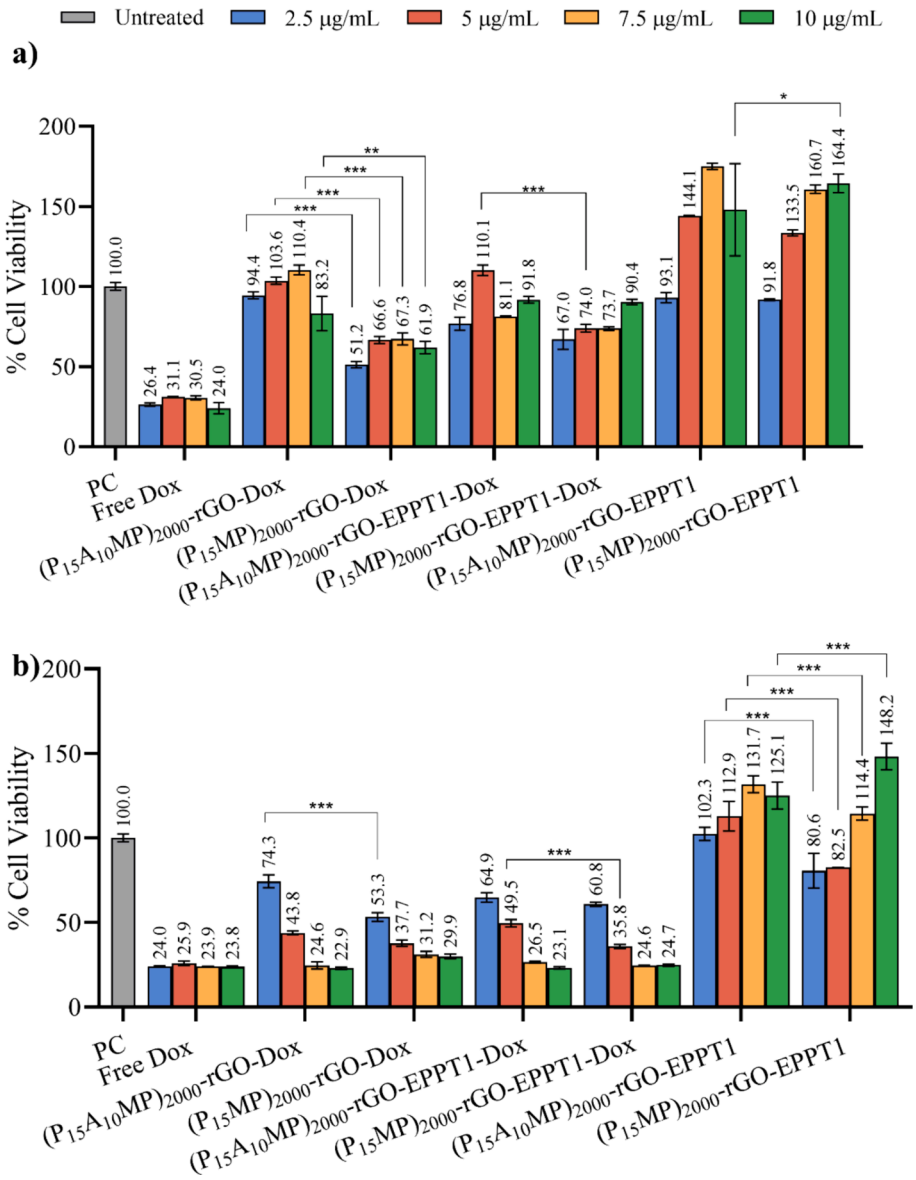

Fig. 8. Resazurin assay results of $(P_{15}A_{10}MP)_{2000}$ derivatives on MCF-7 cancer cell line after **a)** 24 h and **b)** 48 h of incubation. The plotted values represent the mean ± SEM of three independent experiments. Statistical significances are indicated as $p < 0.033$ (*), $p < 0.002$ (**), and $p < 0.001$ (***).

retention effect.

Since PEG_{500} containing PAMP copolymer compositions do not disperse in the water as effectively as PEG_{2000}-containing PAMP, reduction in the cell viability was not measured as clearly as PEG_{2000}-containing compositions; however, a trend proportional to the drug release profile was observed (Fig. 9). $(P_{26}A_{10}MP)_{500}$-rGO-Dox was used to release more drugs than $(P_{26}MP)_{500}$-rGO-Dox within the same time frame, which resulted in better anticancer activity by killing more cancer cells (~60 %), especially after 48 h incubation Fig. 9**b**. Since the effect of PEG chain length and density on drug release is not as dominant as PEG_{2000}-rGO derivatives, azide group contribution can be seen more clearly for PEG_{500}-rGO derivatives. Similarly, the differences in the cell viability of the azide-containing and non-containing targeted carrier became more visible over 48 h because $(P_{26}A_{16}MP)_{500}$-rGO-Dox-EPPT1 was faster than $(P_{26}MP)_{500}$-rGO-Dox-EPPT1 for this time point (Fig. 9**b**).

Selective cellular internalization of EPPT1 peptide targeted carriers was assessed using flow cytometry (Fig. 10**a**) and confocal microscopy (Fig. 10**b**) on the MCF-7 cancer cell line due to its higher uMUC-1 expression [54].

Flow cytometric analysis was performed based on Dox fluorescence intensity of free Dox, targeted ($(P_{15}MP)_{2000}$-rGO-EPPT1-Dox), and non-targeted ($(P_{15}MP)_{2000}$-rGO-Dox) nanoplatform. The results in Fig. 10**a** showed that Dox through diffusion can internalize more into the cells followed by the targeted $(P_{15}MP)_{2000}$-rGO-EPPT1-Dox which has more incidence than its non-targeted $(P_{15}MP)_{2000}$-rGO-Dox version. Further, confocal microscope imaging was performed to visualize the selective cellular entry for targeted carriers on MCF-7 cells. Cell nuclei were colored in blue using Hoechst, and Dox fluorescence was visualized in red (Fig. 10**b**). Free Dox as a small drug molecule can pass the cell membrane through diffusion and accumulate in the nucleus over time, which can be clearly seen in the first row of Fig. 10**b**, especially in the merged picture. When targeted $(P_{15}MP)_{2000}$-rGO-EPPT1-Dox and non-targeted $(P_{15}MP)_{2000}$-rGO-Dox compositions were compared, enhanced uptake of targeted composition was evidenced with increased fluorescence intensity of Dox in the cell. The flow cytometry and confocal microscopy results collectively showed that the EPPT1-conjugated targeted drug-carrying nanoplatform has a better ability for cellular internalization.

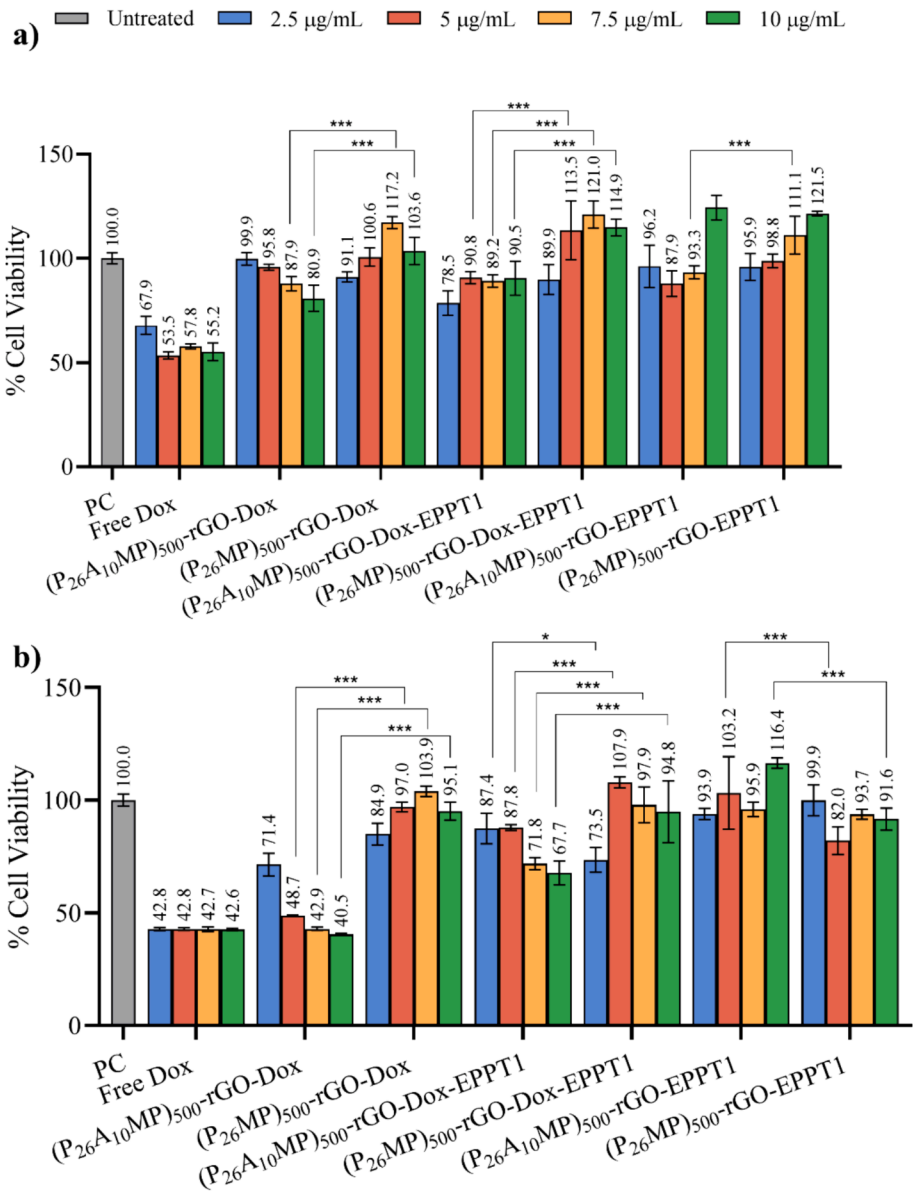

Fig. 9. Resazurin assay results of $(P_{26}A_{10}MP)_{500}$ derivatives on MCF-7 cell line after **a)** 24 h and **b)** 48 h of incubation. The plotted values represent the mean ± SEM of three independent experiments. Statistical significances are indicated as $p < 0.033$ (*), $p < 0.002$ (**), and $p < 0.001$ (***).

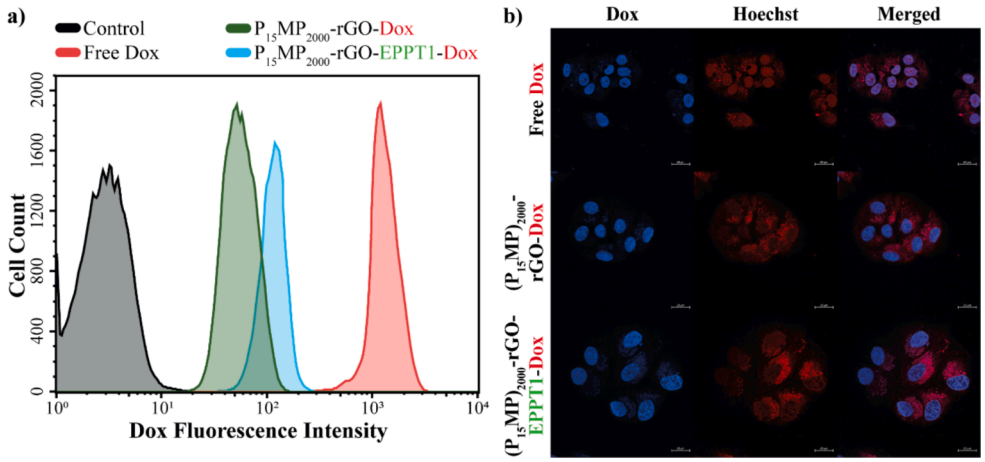

Fig. 10. Cellular uptake analysis of free Dox, $(P_{15}MP)_{2000}$-rGO-Dox, and $(P_{15}MP)_{2000}$-rGO-EPPT1-Dox by **a)** FACS analysis and **b)** confocal microscopy using MCF-7 cells.

4. Conclusions

Herein, a detailed study was conducted to show the effect of the components of well-established PEGylation method on to obtained rGO-based nanoplatform. Azide-functional, well-defined PAMP copolymers were used for PEGylation of GO and simultaneously reduced to azide-containing PEGylated rGO, which was used as a functional nanoplatform to conjugate targeting agent and load the anticancer drug. The effect of the ionic azide group on drug release was investigated by changing the number of azides in the copolymer and comparing it with azide-containing and azide-capped versions of the same copolymer. PEG chain lengths of 500 and 2000 Da were compared with different PEG densities. Finally, a peptide-based targeting agent was conjugated before and after drug loading to see the effect of the conjugation order. The pH-dependent drug release profile showed that the presence of the azide group in the copolymer enhanced the drug release. This behavior was noticeable when higher number of shorter PEG brushes were used for PEGylation since shorter PEG has partial coverage on the surface and allow Dox to interact more with the rGO surface that can feel the presence of ionic azide groups. In the case of longer PEG brush containing composition, azide group effect was able to visible for only less number of PEG brush otherwise dense PEG coating with hydrated layer provide accommodation for Dox more than rGO surface and diminishes the release. Finally, results showed that conjugation peptide-based targeting agents after drug loading slowed down the drug release at acidic pH due to not only EPPT1 peptide coming with additional PEG chains but also the lipophilic character of peptide changes the hydrophilicity of the surface. Neutral pH values in all targeted compositions had a drug release percentage of less than 9.5 %, indicating safety during blood circulation. Given the fact that these nanoplatforms are rGO-based and have strong π-π interaction with the drug, obtained 26–49 % release is acceptable compared to the literature. It can be improved by playing with the PEG chain length, density, and PEGylation components.

CRediT authorship contribution statement

Ezgi Basavci: Visualization, Validation, Methodology, Investigation. **Erhan Demirel:** Visualization, Validation, Methodology, Investigation. **Mohamad Elhassan:** Visualization, Validation, Methodology. **Yasemin Yuksel Durmaz:** Writing – review & editing, Writing – original draft, Supervision, Methodology, Funding acquisition, Conceptualization.

Declaration of competing interest

The authors declare that they have no known competing financial interests or personal relationships that could have appeared to influence the work reported in this paper.

Data availability

Data will be made available on request.

Acknowledgment

The authors (E.B., E.D., and Y.Y.D.) thank The Scientific & Technological Research Council of Turkey (TUBITAK)) for the financial support of this work (Project No: 116Z534). Y.Y.D. also thanks the Turkish Academy of Science for its support through the Outstanding Young Scientist Award (GEBIP) Program.

Appendix A. Supplementary material

Supplementary data to this article can be found online at https://doi.org/10.1016/j.eurpolymj.2024.113211.

References

[1] K.S. Novoselov, A.K. Geim, S.V. Morozov, D. Jiang, Y. Zhang, S.V. Dubonos, I. V. Grigorieva, A.A. Firsov, Electric field in atomically thin carbon films, Science 306 (2004) 666–669, https://doi.org/10.1126/science.1102896.
[2] N.A. Savostianova, S.A. Mikhailov, N. Kumar, J. Kumar, C. Gerstenkorn, R. Wang, H.-Y. Chiu, A.L. Smirl, H. Zhao, 8 T Gu, N. Petrone, J.F. Mcmillan, A. Van Der Zande, M. Yu, G.Q. Lo, D.L. Kwong, J. Hone, C.W. Wong, Third harmonic generation from graphene lying on different substrates: optical-phonon resonances and interference effects " Third harmonic generation in graphene and few-layer graphite films, Phys. Rev. B Phys. Rev. X Prog. Electromag. Res. OPTICS EXPRESS (2013). doi: 10.1364/OE.25.003268.
[3] E. Khakpour, S. Salehi, S.M. Naghib, S. Ghorbanzadeh, W. Zhang, Graphene-based nanomaterials for stimuli-sensitive controlled delivery of therapeutic molecules, Front. Bioeng. Biotechnol. 11 (2023) 1129768, https://doi.org/10.3389/fbioe.2023.1129768.
[4] M. Tavakoli, R. Emadi, H. Salehi, S. Labbaf, J. Varshosaz, Incorporation of graphene oxide as a coupling agent in a 3D printed polylactic acid/hardystonite nanocomposite scaffold for bone tissue regeneration applications, Int. J. Biol. Macromol. 253 (2023) 126510, https://doi.org/10.1016/j.ijbiomac.2023.126510.
[5] M. Tavakoli, H. Salehi, R. Emadi, J. Varshosaz, S. Labbaf, A.M. Seifalian, F. Sharifianjazi, M. Mirhaj, 3D printed polylactic acid-based nanocomposite scaffold stuffed with microporous simvastatin-loaded polyelectrolyte for craniofacial reconstruction, Int. J. Biol. Macromol. 258 (2024) 128917, https://doi.org/10.1016/j.ijbiomac.2023.128917.
[6] Z. Liu, J.T. Robinson, X. Sun, H. Dai, PEGylated nanographene oxide for delivery of water-insoluble cancer drugs, J. Am. Chem. Soc. 130 (2008) 10876–10877, https://doi.org/10.1021/ja803688x.
[7] K. Yang, L. Feng, H. Hong, W. Cai, Z. Liu, Preparation and functionalization of graphene nanocomposites for biomedical applications, Nat. Protoc. 8 (2013) 2392–2403, https://doi.org/10.1038/nprot.2013.146.
[8] A.N. Ghulam, O.A.L. Dos Santos, L. Hazeem, B. Pizzorno Backx, M. Bououdina, S. Bellucci, Graphene oxide (GO) materials—Applications and toxicity on living organisms and environment, JFB 13 (2022) 77, https://doi.org/10.3390/jfb13020077.
[9] A. Rhazouani, H. Gamrani, M. El Achaby, K. Aziz, L. Gebrati, M.S. Uddin, F. Aziz, Synthesis and toxicity of graphene oxide nanoparticles: A literature review of in vitro and in vivo studies, Biomed. Res. Int. 2021 (2021) 1–19, https://doi.org/10.1155/2021/5518999.
[10] J. Liu, L. Tao, W. Yang, D. Li, C. Boyer, R. Wuhrer, F. Braet, T.P. Davis, Synthesis, characterization, and multilayer assembly of pH sensitive graphene-polymer nanocomposites, Langmuir 26 (2010) 10068–10075, https://doi.org/10.1021/la1001978.
[11] J. Liu, L. Cui, D. Losic, Graphene and graphene oxide as new nanocarriers for drug delivery applications, Acta Biomater. 9 (2013) 9243–9257, https://doi.org/10.1016/j.actbio.2013.08.016.
[12] J. Liu, W. Yang, L. Tao, D. Li, C. Boyer, T.P. Davis, Thermosensitive graphene nanocomposites formed using pyrene-terminal polymers made by RAFT polymerization, J. Polym. Sci. Part A: Polym. Chem. (2010), https://doi.org/10.1002/pola.23802.
[13] W. Yu, L. Sisi, Y. Haiyan, L. Jie, Progress in the functional modification of graphene/graphene oxide: A review, RSC Adv. 10 (2020) 15328–15345, https://doi.org/10.1039/D0RA01068E.
[14] R. Justin, B. Chen, Strong and conductive chitosan–reduced graphene oxide nanocomposites for transdermal drug delivery, J. Mater. Chem. B 2 (2014) 3759, https://doi.org/10.1039/c4tb00390j.
[15] N. Pramanik, S. Ranganathan, S. Rao, K. Suneet, S. Jain, A. Rangarajan, S. Jhunjhunwala, A composite of hyaluronic acid-modified graphene oxide and iron oxide nanoparticles for targeted drug delivery and magnetothermal therapy, ACS Omega 4 (2019) 9284–9293, https://doi.org/10.1021/acsomega.9b00870.
[16] S. Zhang, K. Yang, L. Feng, Z. Liu, In vitro and in vivo behaviors of dextran functionalized graphene, Carbon 49 (2011) 4040–4049, https://doi.org/10.1016/j.carbon.2011.05.056.
[17] S. Sattari, M. Adeli, S. Beyranvand, M. Nemati, Functionalized graphene platforms for anticancer drug delivery, IJN 16 (2021) 5955–5980, https://doi.org/10.2147/IJN.S249712.
[18] D.J. Joshi, J.R. Koduru, N.I. Malek, C.M. Hussain, S.K. Kailasa, Surface modifications and analytical applications of graphene oxide: A review, TrAC Trends Anal. Chem. 144 (2021) 116448, https://doi.org/10.1016/j.trac.2021.116448.
[19] P. Orsu, A. Koyyada, Recent progresses and challenges in graphene based nano materials for advanced therapeutical applications: a comprehensive review, Mater. Today Commun. 22 (2020) 100823, https://doi.org/10.1016/j.mtcomm.2019.100823.
[20] X. Zhao, K. Tian, T. Zhou, X. Jia, J. Li, P. Liu, PEGylated multi-walled carbon nanotubes as versatile vector for tumor-specific intracellular triggered release with enhanced anti-cancer efficiency: Optimization of length and PEGylation degree, Colloids Surf. B Biointerfaces 168 (2018) 43–49, https://doi.org/10.1016/j.colsurfb.2018.02.041.
[21] X. Li, H. Jiang, N. He, W.-E. Yuan, Y. Qian, Y. Ouyang, Graphdiyne-Related Materials in Biomedical Applications and Their Potential in Peripheral Nerve Tissue Engineering, Cyborg Bionic Syst 2022 (2022) 2022/9892526. doi: 10.34133/2022/9892526.
[22] E. Demirel, E. Karaca, Y. Yuksel Durmaz, Effective PEGylation method to improve biocompatibility of graphene derivatives, Eur. Polym. J. 124 (2020) 109504, https://doi.org/10.1016/j.eurpolymj.2020.109504.

[23] K. Miyata, R.J. Christie, K. Kataoka, Polymeric micelles for nano-scale drug delivery, React. Funct. Polym. 71 (2011) 227–234, https://doi.org/10.1016/j.reactfunctpolym.2010.10.009.
[24] B. Cengiz, R. Sanyal, A. Sanyal, Tailoring aqueous dispersibility and biofunctionalization of carbon nanotubes using maleimide-containing clickable polymers, ACS Appl. Polym. Mater. (2021), https://doi.org/10.1021/acsapm.1c00977.
[25] E. Demirel, Y. Yuksel Durmaz, PEGylated reduced graphene oxide as nanoplatform for targeted gene and drug delivery, Eur. Polym. J. 186 (2023) 111841, https://doi.org/10.1016/j.eurpolymj.2023.111841.
[26] M. Alibolandi, M. Mohammadi, S.M. Taghdisi, M. Ramezani, K. Abnous, Fabrication of aptamer decorated dextran coated nano-graphene oxide for targeted drug delivery, Carbohydr. Polym. 155 (2017) 218–229, https://doi.org/10.1016/j.carbpol.2016.08.046.
[27] D. Chai, B. Hao, R. Hu, F. Zhang, J. Yan, Y. Sun, X. Huang, Q. Zhang, H. Jiang, Delivery of oridonin and methotrexate via PEGylated graphene oxide, ACS Appl. Mater. Interfaces 11 (2019) 22915–22924, https://doi.org/10.1021/acsami.9b03983.
[28] L. Wang, D. Yu, R. Dai, D. Fu, W. Li, Z. Guo, C. Cui, J. Xu, S. Shen, K. Ma, PEGylated doxorubicin cloaked nano-graphene oxide for dual-responsive photochemical therapy, Int. J. Pharm. 557 (2019) 66–73, https://doi.org/10.1016/j.ijpharm.2018.12.037.
[29] H. Xu, M. Fan, A.M.A. Elhissi, Z. Zhang, K.W. Wan, W. Ahmed, D.A. Phoenix, X. Sun, PEGylated graphene oxide for tumor-targeted delivery of paclitaxel, Nanomedicine (Lond.) 10 (2015) 1247–1262, https://doi.org/10.2217/nnm.14.233.
[30] W. Zhang, Z. Guo, D. Huang, Z. Liu, X. Guo, H. Zhong, Synergistic effect of chemo-photothermal therapy using PEGylated graphene oxide, Biomaterials 32 (2011) 8555–8561, https://doi.org/10.1016/j.biomaterials.2011.07.071.
[31] M. Mahdavi, A. Fattahi, E. Tajkhorshid, S. Nouranian, Molecular insights into the loading and dynamics of doxorubicin on PEGylated graphene oxide nanocarriers, ACS Appl. Bio Mater. 3 (2020) 1354–1363, https://doi.org/10.1021/acsabm.9b00956.
[32] A. Moore, Z. Medarova, A. Potthast, G. Dai, In vivo targeting of underglycosylated MUC-1 tumor antigen using a multimodal imaging probe, Cancer Res. 64 (2004) 1821–1827, https://doi.org/10.1158/0008-5472.CAN-03-3230.
[33] J.I. Paredes, S. Villar-Rodil, A. Martínez-Alonso, J.M.D. Tascón, A. Martinez-Alonso, J.M. Tascon, Graphene oxide dispersions in organic solvents, Langmuir 24 (2008) 10560–10564, https://doi.org/10.1021/la801744a.
[34] W. Zhu, J. Long, M. Shi, Release kinetics model fitting of drugs with different structures from viscose fabric, Materials 16 (2023) 3282, https://doi.org/10.3390/ma16083282.
[35] Z. Medarova, L. Rashkovetsky, P. Pantazopoulos, A. Moore, Multiparametric monitoring of tumor response to chemotherapy by noninvasive imaging, Cancer Res. 69 (2009) 1182–1189, https://doi.org/10.1158/0008-5472.CAN-08-2001.
[36] Y. Oz, A. Barras, R. Sanyal, R. Boukherroub, S. Szunerits, A. Sanyal, Functionalization of reduced graphene oxide via thiol-maleimide “Click” chemistry: Facile fabrication of targeted drug delivery vehicles, ACS Appl. Mater. Interfaces 9 (2017) 34194–34203, https://doi.org/10.1021/acsami.7b08433.
[37] W. Zhang, J. Ma, D. Gao, Y. Zhou, C. Li, J. Zha, J. Zhang, Preparation of amino-functionalized graphene oxide by Hoffman rearrangement and its performances on polyacrylate coating latex, Prog. Org. Coat. 94 (2016) 9–17, https://doi.org/10.1016/j.porgcoat.2016.01.013.
[38] Y.A. Cheon, J.H. Bae, B.G. Chung, Reduced graphene oxide nanosheet for chemo-photothermal therapy, Langmuir 32 (2016) 2731–2736, https://doi.org/10.1021/acs.langmuir.6b00315.
[39] B. Khezri, S.M. Beladi Mousavi, L. Krejčová, Z. Heger, Z. Sofer, M. Pumera, Ultrafast electrochemical trigger drug delivery mechanism for nanographene micromachines, Adv. Funct. Mater. 29 (2019) 1806696, https://doi.org/10.1002/adfm.201806696.
[40] S.Y. Qin, J. Feng, L. Rong, H.Z. Jia, S. Chen, X.J. Liu, G.F. Luo, R.X. Zhuo, X. Z. Zhang, Theranostic GO-based nanohybrid for tumor induced imaging and potential combinational tumor therapy, Small 10 (2014) 599–608, https://doi.org/10.1002/smll.201301613.
[41] W. Zhang, J. Dai, G. Zhang, Y. Zhang, S. Li, D. Nie, Photothermal/pH dual-responsive drug delivery system of amino-terminated HBP-modified rGO and the chemo-photothermal therapy on tumor cells, Nanoscale Res. Lett. 13 (2018), https://doi.org/10.1186/s11671-018-2787-8.
[42] A.H. Hung, R.J. Holbrook, M.W. Rotz, C.J. Glasscock, N.D. Mansukhani, K. W. Macrenaris, L.M. Manus, M.C. Duch, K.T. Dam, M.C. Hersam, T.J. Meade, Graphene oxide enhances cellular delivery of hydrophilic small molecules by co-incubation, ACS Nano 8 (2014) 10168–10177, https://doi.org/10.1021/nn502986e.
[43] K. Taylor, T.A. Tabish, R.J. Narayan, Drug release kinetics of DOX-loaded graphene-based nanocarriers for ovarian and breast cancer therapeutics, Appl. Sci. 11 (2021) 11151, https://doi.org/10.3390/app112311151.
[44] P. Costa, J.M. Sousa Lobo, Modeling and comparison of dissolution profiles, Eur. J. Pharm. Sci. 13 (2001) 123–133, https://doi.org/10.1016/S0928-0987(01)00095-1.
[45] S. Dash, P.N. Murthy, L. Nath, P. Chowdhury, Kinetic modeling on drug release from controlled drug delivery systems, Acta Pol. Pharm. 67 (2010) 217–223.
[46] R.W. Korsmeyer, R. Gurny, E. Doelker, P. Buri, N.A. Peppas, Mechanisms of solute release from porous hydrophilic polymers, Int. J. Pharm. 15 (1983) 25–35, https://doi.org/10.1016/0378-5173(83)90064-9.
[47] T. Higuchi, Rate of release of medicaments from ointment bases containing drugs in suspension, J. Pharm. Sci. 50 (1961) 874–875, https://doi.org/10.1002/jps.2600501018.
[48] X. Yang, X. Zhang, Z. Liu, Y. Ma, Y. Huang, Y. Chen, High-efficiency loading and controlled release of doxorubicin hydrochloride on graphene oxide, J. Phys. Chem. C 112 (2008) 17554–17558, https://doi.org/10.1021/jp806751k.
[49] H. Hu, J. Yu, Y. Li, J. Zhao, H. Dong, Engineering of a novel pluronic F127/graphene nanohybrid for pH responsive drug delivery, Journal of Biomedical Materials Research - Part A 100 A (2012) 141–148. doi: 10.1002/jbm.a.33252.
[50] T.T. Pham, H.T. Nguyen, C.D. Phung, S. Pathak, S. Regmi, D.-H. Ha, J.O. Kim, C. S. Yong, S.K. Kim, J.-E. Choi, S. Yook, J.-B. Park, J.-H. Jeong, Targeted delivery of doxorubicin for the treatment of bone metastasis from breast cancer using alendronate-functionalized graphene oxide nanosheets, J. Ind. Eng. Chem. 76 (2019) 310–317, https://doi.org/10.1016/j.jiec.2019.03.055.
[51] D. Depan, J. Shah, R.D.K.K. Misra, Controlled release of drug from folate-decorated and graphene mediated drug delivery system: Synthesis, loading efficiency, and drug release response, Mater. Sci. Eng. C 31 (2011) 1305–1312, https://doi.org/10.1016/j.msec.2011.04.010.
[52] P. Thulasiraman, A.B. Johnson, Regulation of Mucin 1 and multidrug resistance protein 1 by honokiol enhances the efficacy of doxorubicin-mediated growth suppression in mammary carcinoma cells, Int. J. Oncol. (2016) 8.
[53] D. Chow, M.L. Nunalee, D.W. Lim, A.J. Simnick, A. Chilkoti, Peptide-based biopolymers in biomedicine and biotechnology, Mater. Sci. Eng. R. Rep. 62 (2008) 125–155, https://doi.org/10.1016/j.mser.2008.04.004.
[54] M.D. Walsh, S.M. Luckie, M.C. Cummings, T.M. Antalis, M.A. McGuckin, Heterogeneity of MUC1 expression by human breast carcinoma cell lines in vivo and in vitro, Breast Cancer Res. Treat. 58 (1999) 255–266, https://doi.org/10.1023/a:1006345301364.